Ductular reaction-associated neutrophils promote biliary epithelium proliferation in chronic liver disease

Silvia Ariño[1,3+], Beatriz Aguilar-Bravo[1+], Mar Coll[1,2,3+*], Woo-Yong Lee[4], Moritz Peiseler[4], Paula Cantallops[1], Laura Sererols-Viñas[1], Raquel A Martínez-García de la Torre[1], Celia Martínez-Sánchez[1,3], Jordi Pedragosa[1,7], Laura Zanatto[1], Jordi Gratacós-Ginès[1,5], Elisa Pose[1,2,3,5], Delia Blaya[1], Xènia Almodóvar[1], María Fernández-Fernández[1,6], Paloma Ruiz-Blázquez[1,6], Juan José Lozano[3], Silvia Affo[1,3], Anna M Planas[1,7], Pere Ginès[1,3,5], Anna Moles[1,6], Paul Kubes[4¥] and Pau Sancho-Bru[1,2,3¥*].

*Corresponding authors

+ These authors are first co-authors and equally contributed to this work

¥ These authors are co-main author of this study

[1]Institut d'Investigacions Biomèdiques August Pi i Sunyer (IDIBAPS), Barcelona, Spain.

[2] Medicine Department, Faculty of Medicine, University of Barcelona, Barcelona, Spain.

[3] Centro de Investigación Biomédica en Red de Enfermedades Hepáticas y Digestivas (CIBERehd), Barcelona, Spain.

[4] Snyder Institute for Chronic Diseases, University of Calgary, Calgary, Alberta, Canada.

[5]Liver Unit, Hospital Clínic, Faculty of Medicine, University of Barcelona, Barcelona, Spain.

[6]Cell Death and Proliferation, Institute of Biomedical Research of Barcelona, Spanish National Research Council, Barcelona, Spain.

[7]Department of Brain Ischemia and Neurodegeneration, Institut d'Investigacions Biomèdiques de Barcelona (IIBB), Consejo Superior de Investigaciones Científicas (CSIC), Barcelona, Spain.

Correspondence to:

Pau Sancho-Bru, PhD; Institut d'Investigacions Biomèdiques August Pi i Sunyer (IDIBAPS); Centre Esther Koplowitz, C/ Rosselló, 149-153, third floor; 08036 Barcelona, Spain; **psancho@recerca.clinic.cat**

Mar Coll, PhD; Medicine Department, Faculty of Medicine, University of Barcelona, Barcelona, Spain; Centre Esther Koplowitz, C/ Rosselló, 149-153, third floor; 08036 Barcelona, Spain; **marcoll@ub.edu**

Keywords: Ductular reaction, biliary cells, neutrophils, chronic injury, elastase, neutrophil extracellular traps, organoids

Data availability statement: RNA-sequencing datasets generated in this paper are available under GEO accession code: GSE203336.

Financial support: This work has been supported by grants from Fondo de Investigación Sanitaria Carlos III (FIS), co-financed by Fondo Europeo de Desarrollo Regional (FEDER), Unión Europea, "Una manera de hacer Europa" (FIS PI20/00765 to P.S.-B and FIS 18-PI18/00862 to M.C), from the NIH National

Institute on Alcohol Abuse and Alcoholism grant 1U01AA021908-01-33490 to P.S.-B. P.G. is funded by Agencia de Gestió d'Ajuts Universitaris i de Recerca (AGAUR) 2014 SGR 708, Centro de Investigación en Red Enfermedades Hepáticas y Digestivas (CIBERehd) and Institució Catalana de Recerca i Estudis Avançats (ICREA). MC is funded by Ramon y Cajal programme from the Ministerio de Ciencia e Innovación RYC2019-026662-I and by Plan estatal de investigación científica y técnica de innovación PID2021-125195OB-I00. S.A received a grant from the Ministerio de Educación, Cultura y Deporte, FPU programme (FPU17/04992). B.A.-B. is funded by Instituto de Salud Carlos III, PFIS (FI16/00203) and MC is funded by Ramon y Cajal programme from the Ministerio de Ciencia e Innovación RYC2019-026662-I.

Author contributions: SA and BA-B participated in the design of this study, performed experiments and drafted the manuscript; MC participated in the design of this study, performed and supervised experiments and critically reviewed the manuscript; W-YL and MP performed spinning disk intravital experiments. PC and LZ contributed to organoid experiments. DB, LS-V, RAM-G and CM-S contributed to animal experiments and critically reviewed the manuscript. EP and JG-G recruited patients for the study and contributed to the critical review of the manuscript. JP, XA, MF-F and PR-B contributed to histological analysis. JJL performed bioinformatics analysis. AM, SA, AMP and PG interpreted data and contributed to the critical review of the manuscript; PK and P S-B conceived and designed the study, critically reviewed the manuscript and supervised the study.

ABSTRACT

Background & aims: Ductular reaction expansion is associated with poor prognosis in patients with advanced liver disease. However, the mechanisms promoting biliary cell proliferation are largely unknown. Here we identify neutrophils as drivers of biliary cell proliferation and defective wound-healing response.

Methods: Liver tissue location of neutrophil was evaluated in patients with chronic liver disease. Neutrophil dynamics was analyzed by intravital microscopy and neutrophil-labeling assays in DDC treated mice. Neutrophil depletion or recruitment inhibition was achieved using Ly6g antibody and CXCR1/2 inhibitor, respectively. Mice deficient in PAD4 and neutrophil elastase (NE) were used to investigate the mechanisms underlying ductular reaction expansion.

Results: In this study we describe a population of ductular reaction-associated neutrophils (DRANs), which are in direct contact to the biliary epithelial cells in chronic liver diseases and their number increases along disease progression. We show that DRANs are immobilized at the ductular reaction for a prolonged period of time. In addition, liver neutrophils display a unique phenotypic and transcriptomic profile, showing a decreased phagocytic capacity and increased oxidative burst. Depletion of neutrophils or inhibition of their recruitment reduces DRANs and the expansion of ductular reaction, while mitigating liver fibrosis and angiogenesis. Mechanistically, neutrophils deficient in PAD4 and NE abrogate neutrophil-induced biliary cell proliferation, thus indicating the role of neutrophil extracellular traps and elastase release in ductular reaction expansion.

Conclusions: Overall, our study reveals the accumulation of DRANs as a hallmark of advanced liver disease and a potential therapeutic target to mitigate ductular reaction and maladaptive wound-healing response.

Impact and implications: Our results indicate that neutrophils are highly plastic and can have an extended lifespan. Moreover, we identify a new role of neutrophils as triggers of expansion of the biliary epithelium. Overall, the results of this study indicate that ductular reaction-associated neutrophils (DRANs) are new players in maladaptive tissue healing response in chronic liver injury and may be a potential target for therapeutic interventions to reduce ductular reaction expansion and promoting tissue repair in advanced liver disease.

INTRODUCTION

Ductular reaction is a maladaptive regenerative response of the liver taking place in advanced chronic liver diseases. Ductular reaction release pro-inflammatory mediators that lead to neutrophil recruitment[1–3], lymphocyte accumulation[4,5], hepatic stellate cell activation[6,7] and new vessel formation[8], thus contributing to abnormal wound-healing response. In advanced chronic liver diseases, ductular reaction expansion is associated with disease progression and patients' poor outcome[9–11].

Neutrophils are the first line of defense against pathogens and infection but they also play important functions in tissue response to injury in both acute and chronic injury conditions [13–16]. In acute sterile liver injury, recruited neutrophils perform key restorative functions and return to the circulation migrating back to the bone marrow[12,17]. However, neutrophil recruitment and function in chronic liver injury is still largely unexplored.

Chronic liver diseases have an important effect on circulating neutrophil function, which show reduced phagocytic capacity and superoxide production [18–20]. Recruited neutrophils are associated with increased liver injury, cholestasis and portal hypertension [3,21,22], and the secretion of hydrolytic and oxidative molecules exacerbates tissue injury [23–26].

Although infiltrating neutrophils to the injured liver is a common histological feature in advanced liver diseases, little is known about their recruitment dynamics, phenotype and role in liver wound-healing. In this study, we describe ductular reaction-associated neutrophils (DRANs), which accumulate at the biliary epithelium cells and display altered dynamics, phenotype and function. We show that neutrophils mediate biliary epithelium proliferation, contributing to

maladaptive wound-healing response. These findings suggest that targeting DRANs may be an appealing approach to promote an effective wound-healing response in liver disease.

MATERIALS AND METHODS

Patients

Liver paraffin-embedded sections of biopsies from patients with alcohol-related liver disease (ALD) admitted to the Liver Unit of the Hospital Clinic of Barcelona were used. Signed informed consent was obtained from all the patients, and the study was approved by the Ethics Committee of the Hospital Clinic. The ALD cohort included patients in different disease stages: pre-cirrhosis (n=5, F2-F3), compensated cirrhosis (n=5, F4), decompensated cirrhosis (n=5, F4) and alcohol-related hepatitis (AH) (n=5, F4).

Animal models

12-week-old C57BL/6J mice (Charles River) were fed with 0.1% 3,5-diethoxycarbonyl-1,4-dihydro-collidin (DDC) (Sigma-Aldrich, St. Louis, MO) standard diet. 1-week DDC treatment, carbon tetrachloride injury model and isolation of control mice cells were performed using both male and female mice whereas long-term treatment of 3 weeks of DDC and bile-duct ligation were performed in male mice. Inhibition of CXCR1/2 receptor activity was performed with SCH-527123 (MedChemExpress) and neutrophil depletion was achieved by anti-Ly6G (1A8) antibody (BioXcell) administration. Neutrophil elastase and protein arginine deiminase 4 deficient mice ($NE^{-/-}$ and $PAD4^{-/-}$) were obtained from Jackson Laboratory. All animal experiments were approved by the Ethics Committee of Animal Experimentation of the University of Barcelona. See supplementary data for details.

Data availability

The authors declare that all data supporting the findings of this study are available within the article and its Supplementary information files or from the

corresponding author upon request. Raw RNA-seq data have been deposited in the Gene Expression Omnibus (GEO) database under accession code GSE203336.

All the other material and methods are described in the Supplementary Data.

RESULTS

Neutrophils are immobilized at the biliary epithelium in advanced chronic liver disease.

We first determined the localization of infiltrating neutrophils in liver samples from patients with chronic liver disease. In advanced chronic liver diseases, neutrophils were predominantly recruited at the periportal area and were closely associated with KRT7^{+} ductular reaction biliary cells in all the examined etiologies, including hepatitis C and B virus, non-alcoholic fatty liver disease, alcohol-related liver disease and primary biliary cholangitis (Fig. 1A and Supplementary Fig. 1A). This observation suggests that the presence of ductular reaction-associated neutrophils, which we named DRANs, is a common feature in advanced liver diseases, independently of the cause or etiology. Moreover, we found that the extent of DRANs and their proximity to the ductular reaction increases with disease progression and correlate with ductular reaction expansion (Fig. 1B and Supplementary Fig. 1B). Liver tissue clearing from patients with advanced chronic liver disease showed that DRANs are in cell contact with biliary epithelial cells (Fig. 1C and Supplementary Video 1).

To evaluate the dynamic behavior of DRANs, we tracked neutrophils *in vivo* in mice treated with DDC diet [27]. In DDC-treated mice (1 and 3 weeks of diet) neutrophils were located at the ductular reaction (73,3%±1,76) rather than within the sinusoids in the central area (Supplementary Fig. 1A and 1C). Intravital microscopy analysis revealed that DRANs surrounded the network of EpCAM^{+} biliary epithelial cells (Fig. 1D). Moreover, 3D reconstruction of Z-stack images showed that DRANs are in close contact with EpCAM^{+} cells (Fig. 1E and Supplementary Video 2). On the contrary, neutrophils were rarely seen at the

central area or at sinusoids (Fig. 1D). The accumulation of DRANs at the biliary epithelium structures was confirmed in bile-duct ligated mice as a second cholestatic experimental model (Supplementary Fig. 1E and 1F). On the contrary, in CCl4 mouse model model, which has mild ductular reaction, neutrophils were found at the central area (Supplementary Fig. 1F). Neutrophil recruitment to the liver started as early as two days after DDC diet. Of note, although at day 4 of DDC treatment the number of liver neutrophils slightly increased, there was a prominent change in their location when compared to day 2. At day 4 DRANs appeared closely associated with $EpCAM^+$ cells and their accumulation at ductular reaction increased even further at day 7 of DDC diet (Fig. 1F).

DRANs are long-lasting and show a static behavior.

Next, we aimed to visualize the dynamics of DRANs by using intravital microscopy. A 60-minute-long video of DDC-fed mice show that Ly6G positive neutrophils are located at the ductular reaction displaying a static behavior, with little or no movement (Fig. 2A and Supplementary Video 3). This contrasts the previous work reported in acute liver injury where neutrophils were very dynamic[17]. Acute focal thermal injury on DDC-treated animals induced a rapid recruitment of neutrophils to the site of injury, while the number of DRANs at $EpCAM^+$ cells was unaltered (Fig. 2B and Supplementary Video 4). These data suggest that the sterile injury could not recruit DRANs away from the ductular reaction suggesting an overriding stop signal.

Although neutrophils have a short lifespan in homeostasis, several reports suggest that this can be significantly increased in injury or infection[28]. Thus, to evaluate the retention of DRANs and to track their recruitment and persistence

within the liver tissue, we labeled bone marrow proliferating neutrophils with 5-ethynyl-2'-deoxyuridine (EdU) in DDC-treated mice[29]. At day two after EdU administration, 80% of neutrophils at the bone marrow where positive for EdU, while EdU^+ neutrophils where still not present in circulation or in the liver. The number of labeled neutrophils at the bone marrow peaked at day 3 and declined until day 8. In the blood or in the liver, EdU^+ neutrophils started to be detected at day 3 and reached peak levels at day 4. Interestingly, while circulating EdU^+ neutrophils then declined completely mirroring the decline in bone marrow, the amount of liver EdU^+ neutrophils remained at peak levels and unchanged for a period of three days, suggesting that these cells were not being continuously replaced by new neutrophils, but rather remained immobilized to the $EpCAM^+$ cells. At day 8, EdU^+ liver neutrophils did decline (Fig. 2C and 2D and Supplementary Fig. 2A). Fig. 2E shows a representative image of EdU^+ DRANs at day 5 after EdU injection. This strikingly different kinetics of neutrophils between circulation and the liver tissue reveals that DRANs are retained at the liver and have a prolonged lifespan.

Liver neutrophils in DDC mice adopt a unique phenotypic and functional profile.

Liver neutrophils from DDC mice showed increased CXCR4 and reduced CD62L (L-Selectin) expression when compared to bone marrow or circulating neutrophils (Fig. 3A, 3B and 3C), and $CXCR4^{high}$ liver neutrophils were increased as compared to control mice (Fig. 3D). Based on previous studies, these results indicate that liver neutrophils show an aged-related phenotype [31–33].

RNA-sequencing of Ly6G$^+$ neutrophils isolated from the liver (highly enriched in DRANS, 73,3±1,76%) and blood from DDC mice showed clear differences in their transcriptomic profile (Fig. 3E and Supplementary Fig. 3A). Liver neutrophils were enriched in inflammation and oxidative stress-related pathways and chemokines and chemokine receptors (Fig. 3F and 3G). Flow cytometry analysis confirmed the expression of CCR2, a marker of tissue infiltrating neutrophils [34,35] in liver neutrophils (Fig. 3H). Furthermore, a protein-protein interaction analysis with up-regulated genes in liver neutrophils identified *Tnfa* as central player in neutrophil related inflammatory network (Supplementary Fig. 3B). Genes involved in phagocytosis, degranulation and respiratory burst were altered between liver and blood neutrophils (Fig. 3I). Interestingly, DDC-liver neutrophils showed an enrichment in inflammatory and wound-healing biological processes as compared to control liver neutrophils. These results suggest that neutrophil gene expression profile is altered as a result of injury and infiltration (Supplementary Fig. 3C and 3D).

Next, we functionally evaluated neutrophils from DDC-treated mice. As shown in Fig. 4A and 4B, liver neutrophils showed an increased baseline expression of *Tnfa*, *Cxcl2*, *Il6* and *Il10* and secretion of TNFa and IL-6. In addition, cytokine production upon LPS stimulation was higher in liver neutrophils than in the blood neutrophils (Fig. 4B). Phagocytic capacity and burst index of circulating neutrophils was reduced in DDC-treated mice compared to healthy mice (Supplementary Fig. 4, Fig. 4C and 4D), and was further reduced in DDC liver neutrophils (Fig. 4C). By contrast, burst capacity was increased in DDC liver neutrophils at basal level and after stimulation with phorbol myristate acetate (PMA) when compared with circulating neutrophils (Fig. 4D).

We previously demonstrated the existence of a crosstalk between neutrophils and ductular reaction and described ductular reaction as an important source of CXCL ligands in chronic liver disease[1], thus suggesting that ductular reaction recruits neutrophils and alters their phenotype through CXCR1/2-dependent signaling. To address this hypothesis we used conditioned medium from DDC mice-biliary organoids as an *in vitro* model of ductular reaction [1,8]. First, we observed that organoid conditioned medium induced neutrophil migration, which was abrogated by SCH-527123, a CXCR1/2 inhibitor (Fig. 4E). Neutrophil stimulated with organoid conditioned medium showed lower levels of L-selectin, increased expression of CD11b, CXCR4 and CCR2 and increased expression of *IL6*, *Tnfa*, *Il1b* and *Cxcl1*, mimicking the phenotype observed in DDC mice. This phenotype was partially prevented by SCH-527123 (Fig. 4F and 4G), but CXCR4 and L-selectin expression did not change (Fig. 4G).

Overall, these results indicate that ductular reaction recruit neutrophils and promote changes in their phenotype and function through CXCL-CXCR1/2 axis.

Liver neutrophils promote biliary epithelium cell proliferation and expansion.

To determine the role of neutrophils we 1) depleted neutrophils, and 2) inhibited neutrophil recruitment in DDC mouse model. Depletion of neutrophils with anti-Ly6G antibody, as assessed by MPO and Ly6G staining, resulted in a reduction of the ductular reaction expansion, fibrosis deposition and angiogenesis (Fig. 5A and Supplementary Fig. 5A). Neutrophil depletion reduced the number of SOX9 and EPCAM proliferating cells (Fig. 5B and 5C), which is in agreement with proliferating KRT7 cells in human samples (Supplementary Fig. 1D). The

311 reduction of ductular reaction cells was not associated with increased apoptosis
312 or senescence (Supplementary Fig. 5B). No proliferating endothelial cells or
313 differences in hepatocyte proliferation were observed, suggesting that changes
314 in angiogenesis may be mediated by sprouting and cell mediated processes
315 rather than cell expansion [36] (Supplementary Fig. 5C and 5D). Neutrophil
316 depletion reduced the expression of *Epcam*, but not of inflammatory mediators
317 (Supplementary Fig. 5E). This effect was not due to reduced liver injury, as
318 transaminase serum levels increased after neutrophil depletion (Supplementary
319 Fig. 5F).
320 We have previously shown that ductular reaction cells recruit neutrophils and
321 alter their phenotype through CXCR1/2. Thus, we inhibited *in vivo* neutrophil
322 recruitment with the CXCR1/2 inhibitor SCH-527123. Intravital imaging showed
323 that SCH-527123 reduced the accumulation of DRANs at $EPCAM^{+}$ cells
324 (Supplementary Fig. 6A). Inhibition of CXCR1/2 for 3 weeks in DDC mice (Fig.
325 6A) resulted in a reduction of the expression of pro-inflammatory and pro-
326 fibrogenic mediators as well as biliary markers such as *Epcam* and *Hnf1b*
327 (Supplementary Fig. 6B). CXCR1/2 inhibition reduced DRANs, proliferating
328 ductular reaction cells, the deposition of fibrosis and the degree of intrahepatic
329 angiogenesis (Fig. 6B, 6C and 6D). Apoptosis or senescence was not detected
330 in ductular reaction (Supplementary Fig. 6C). We did not observe ki67+
331 endothelial cells (Supplementary Fig. 6D). Hepatocyte proliferation did not
332 change after SCH-527123 treatment (Supplementary Fig. 6E). No changes in
333 liver injury levels were observed (Supplementary Fig. 6F). These results indicate
334 that CXCR1/2-dependent recruitment of neutrophils lead to ductular reaction
335 expansion.

Neutrophil extracellular traps and neutrophil elastase mediates biliary epithelium expansion.

In chronic liver damage, infiltrating neutrophils release neutrophil extracellular traps (NETs) contributing to liver injury[37–39]. Moreover, NETs have been linked to cell proliferation in tumor development[40]. Mice deficient for peptidyl arginine deiminase 4 (PAD4), a molecule required for histone citrullination and NET formation, were fed with DDC diet. Deficient NETosis in PAD4$^{-/-}$ mice was validated by citrullinated histone H3 and MPO co-staining (Fig. 7A). DDC-treated PAD4$^{-/-}$ mice showed a slight increase in DRANs, but an important reduction ductular reaction expansion and proliferating KRT19+ cells (Fig. 7B, 7C and 7D). However, no expression of cleaved caspase 3 or p21 in ductular reaction cells was observed (Supplementary Fig. 7A). Hepatocyte proliferation increased in PAD4$^{-/-}$ mice, but no Ki67+ endothelial cells were observed (Supplementary Fig. 7B and 7C). To explore whether neutrophil elastase, a NET-associated protease, mediates biliary epithelium expansion, we examined elastase deficient mice (NE$^{-/-}$) fed with DDC for three weeks. No changes in NETosis were observed as assessed by citrullinated histone H3 and MPO co-staining (Fig. 7E). Although liver injury in NE$^{-/-}$ DDC-treated mice was not affected (Supplementary Fig. 7D), we observed a reduction in the expression of fibrosis and progenitor cell genes (Supplementary Fig. 7E). Histologically, NE$^{-/-}$ mice presented no major differences in the number of DRANs but a reduction of proliferating and expansion of ductular reaction cells (Fig. 7F, 7G and 7H). No expression of cleaved caspase 3 and p21 in ductular reaction cells was observed (Supplementary Fig. 7F). While hepatocyte proliferation decreased in NE$^{-/-}$ mice, no proliferation was observed in endothelial cells (Supplementary Fig. 7G and

7H). To provide evidences for a direct effect of neutrophil elastase on ductular reaction proliferation, biliary organoids were co-cultured for 1 week in low-attachment plates with PMA-stimulated neutrophils from control and $NE^{-/-}$ mice. As observed *in vivo* and in liver disease patients, neutrophils increased the proliferation of organoids. Although not totally prevented, the induction of organoid proliferation was lower when elastase-deficient neutrophils were used (Fig. 7I).

Combined, these results indicate that neutrophil elastase promotes biliary epithelium expansion, and therefore may be involved in the maladaptive wound-healing and regenerative response of the liver in the context of chronic liver disease.

DISCUSSION

In this study we describe the complex recruitment dynamics of neutrophils in chronic liver injury and we define DRANs as a distinct population of neutrophils immobilized at the ductular reaction with an extended half-life. Most of the information on the dynamic recruitment of neutrophils to the tissues derives from studies on infection or acute injury. In the healthy liver, neutrophils can be found in the sinusoidal vasculature but very rarely infiltrating the parenchyma. When there is a sterile acute liver insult such as local thermal injury or ischemia-reperfusion, neutrophils are rapidly recruited to the site of damage, where they remain for a short time before returning to the vasculature[17]. In this study we show that the recruitment dynamics of neutrophils in chronic liver injury is different and that a population of neutrophils located at ductular reaction, named DRANs, emerges and persist for several days. This observation suggests that DRANs may have an extended lifespan, with the potential to become a stable inflammatory cell pool.

We show that neutrophil recruitment to the liver entail important changes in their phenotype and function. DRANs adopt an aged phenotype but also start to express receptors that may be important for their intrahepatic recruitment. This is in agreement with studies showing that expression of CCR-family members increase in neutrophils recruited in chronic inflammatory sites[35]. Moreover, we demonstrate that CXCL- chemokines among other soluble factors secreted by ductular reaction participate in neutrophil acquisition of a pro-inflammatory and altered phenotype. As previously reported in the literature, our results evidence the effect of environment tissue factors on neutrophils, driving their adaptation and changes in their phenotype which allow a fine tune recruitment to the tissue

and specialized functions[34,35]. Moreover, aged neutrophil phenotype is associated with the acquisition of a more reactive and inflammatory function[31–33]. These results highlight the plasticity of liver recruited neutrophils and how neutrophils adapt to chronic injury environment. A growing number of studies report the existence of heterogeneity within neutrophil population in different contexts[30,41]. Whether liver neutrophils in chronic injury comprise a heterogeneous population and which phenotypic and functional characteristics define each of these populations require further investigation.

The recruitment of neutrophils in response to infection or acute injury stimulates the secretion of hydrolytic and oxidative molecules at the site of injury, which affect neighboring cells exacerbating tissue injury[23,24,42]. Moreover, the release of NETs also have an impact on the surrounding tissue promoting vascular thrombosis and enhancing inflammatory response[21,39,43]. However, besides the detrimental role of neutrophils to tissue injury, neutrophils have been shown to be able to participate in tissue healing[23,44,45]. Our study expands on the understanding of the role of neutrophils in chronic liver injury and provides evidence that neutrophils are involved in ductular reaction expansion affecting fibrosis and angiogenesis.

We show that DRANs and ductular reaction cells have an important crosstalk. The finding that both $PAD4^{-/-}$ and $NE^{-/-}$ mice showed reduced biliary epithelium cell proliferation but not apoptosis or senescence, indicates that NETosis and specifically, elastase, may be involved in the proliferation of biliary epithelium cells. These results are in agreement with reports describing the role of NETs in triggering cell proliferation in the cancer field where NET-associated proteases NE and MMP9 sequentially cleave the extracellular matrix protein laminin,

promoting proliferation of cancer cells[47]. However, due to the opposite effects observed on biliary cells and hepatocytes, further analyses are required to clarify the cell specific effect of neutrophils in liver regeneration. Besides the role in biliary regeneration, these results expand the concept that neutrophils may functionally interact with epithelial cells regulating their proliferation and therefore may be playing a role in other epithelial tissues.

Here, we describe the dynamics of DRANs in chronic liver injury and their role on the expansion of ductular reaction. We show that neutrophils are plastic and adapt to tissue injury acquiring a new phenotype, function and lifespan. Moreover, we describe that DRANs promote ductular reaction expansion, thus uncovering their role as players in liver regeneration and wound-healing. All these data suggest that neutrophils can be a good therapeutic target to mitigate ductular reaction expansion and to promote liver regeneration and tissue repair in chronic liver diseases.

Abbreviations: AH, alcohol-related hepatitis; ALD, alcohol-related liver disease; ALT, alanine aminotransferase; AP, alkaline phosphatase; AST, aspartate aminotransferase; BDL, bile-duct ligation; CCl4, carbon tetrachloride; CCND1, cyclin D1; CH, cirrhosis; CM, conditioned medium; DDC, 3,5-Diethoxycarbonyl-1,4-dihydrocollidine; DRANs, ductular reaction-associated neutrophils; EdU, 5-ethynyl-2'-deoxyuridine; EPCAM, epithelial cell adhesion molecule; FOV, field of view; GO, gene ontology; HBV, hepatitis B virus; HCV, hepatitis C virus; KRT19, cytokeratin19; KRT7, cytokeratin7; LDH, lactate dehydrogenase; LPS, lipopolysaccharide; MIF, mean intensity fluorescence; MPO, myeloperoxidase;

NASH, non-alcoholic fatty liver disease; NE, neutrophil elastase; PAD4, peptidyl arginine deiminase 4; PBC, primary biliary cholangitis, PCA, principal component analysis; PMA, phorbol 12-myristate 13-acetate; ROS, reactive oxygen species; SD-IVM, spinning-disk confocal intravital microscopy.

Acknowledgments: This work was performed in part at the Centre Esther Koplowitz (CEK) (Barcelona, Spain) and at the Snyder Institute for Chronic Diseases (Calgary, Canada). The authors wish to thank Lori Zbytnuik for her advice and support and Pepa Ros for her excellent laboratory management support. We are indebted to the Biobank Unit and the cytometry and cell sorting facility of Institut d'Investigacions Biomèdiques August Pi i Sunyer (IDIBAPS) for their technical help.

REFERENCES

[1] Aguilar-Bravo B, Rodrigo-Torres D, Ariño S, Coll M, Pose E, Blaya D, et al. Ductular Reaction Cells Display an Inflammatory Profile and Recruit Neutrophils in Alcoholic Hepatitis. Hepatology 2019;69:2180–95. https://doi.org/10.1002/hep.30472.

[2] Govaere O, Cockell S, Van Haele M, Wouters J, Van Delm W, Van den Eynde K, et al. High-throughput sequencing identifies aetiology-dependent differences in ductular reaction in human chronic liver disease. J Pathol 2019;248:66–76. https://doi.org/10.1002/path.5228.

[3] Takeuchi M, Vidigal PT, Guerra MT, Hundt MA, Robert ME, Olave-Martinez M, et al. Neutrophils interact with cholangiocytes to cause cholestatic changes in alcoholic hepatitis. Gut 2021;70:342–56. https://doi.org/10.1136/gutjnl-2020-322540.

[4] Wiggins BG, Pallett LJ, Li X, Davies SP, Amin OE, Gill US, et al. The human liver microenvironment shapes the homing and function of CD4+ T-cell populations. Gut 2022;71:1399–411. https://doi.org/10.1136/GUTJNL-2020-323771.

[5] Zimmer CL, von Seth E, Buggert M, Strauss O, Hertwig L, Nguyen S, et al. A biliary immune landscape map of primary sclerosing cholangitis reveals a dominant network of neutrophils and tissue-resident T cells. Sci Transl Med 2021;13:3107. https://doi.org/10.1126/SCITRANSLMED.ABB3107/SUPPL_FILE/SCITRANSLMED.ABB3107_SM.PDF.

[6] Zhang Z, Zhong X, Shen H, Sheng L, Liangpunsakul S, Lok AS, et al.

Biliary NIK promotes ductular reaction and liver injury and fibrosis in mice. Nat Commun 2022;13:1–15. https://doi.org/10.1038/s41467-022-32575-8.

[7] Williams MJ, Clouston AD, Forbes SJ. Links between hepatic fibrosis, ductular reaction, and progenitor cell expansion. Gastroenterology 2014;146:349–56. https://doi.org/10.1053/j.gastro.2013.11.034.

[8] Coll M, Ariño S, Martínez-Sánchez C, Garcia-Pras E, Gallego J, Moles A, et al. Ductular reaction promotes intrahepatic angiogenesis through Slit2–Roundabout 1 signaling. Hepatology 2022;75:353–68. https://doi.org/10.1002/HEP.32140.

[9] Sancho-Bru P, Altamirano J, Rodrigo-Torres D, Coll M, Millán C, José Lozano J, et al. Liver progenitor cell markers correlate with liver damage and predict short-term mortality in patients with alcoholic hepatitis. Hepatology 2012;55:1931–41. https://doi.org/10.1002/hep.25614.

[10] Roskams T. Liver stem cells and their implication in hepatocellular and cholangiocarcinoma. Oncogene 2006;25:3818–22. https://doi.org/10.1038/SJ.ONC.1209558.

[11] Banales JM, Huebert RC, Karlsen T, Strazzabosco M, LaRusso NF, Gores GJ. Cholangiocyte pathobiology. Nat Rev Gastroenterol Hepatol 2019;16:269–81. https://doi.org/10.1038/S41575-019-0125-Y.

[12] McDonald B, Kubes P. Neutrophils and Intravascular Immunity in the Liver during Infection and Sterile Inflammation. Toxicol Pathol 2011;40:157–65. https://doi.org/10.1177/0192623311427570.

[13] Castanheira FVS, Kubes P. Neutrophils and NETs in modulating acute and chronic inflammation. Blood 2019;133:2178–85. https://doi.org/10.1182/BLOOD-2018-11-844530.

[14] Wang J. Neutrophils in tissue injury and repair. Cell Tissue Res 2018;371:531–9. https://doi.org/10.1007/S00441-017-2785-7.

[15] Casanova-Acebes M, Nicolás-Ávila JA, Li JL, García-Silva S, Balachander A, Rubio-Ponce A, et al. Neutrophils instruct homeostatic and pathological states in naive tissues. J Exp Med 2018;215:2778–95. https://doi.org/10.1084/JEM.20181468.

[16] Mayadas TN, Cullere X, Lowell CA. The Multifaceted Functions of Neutrophils. Annu Rev Pathol 2014;9:181–218. https://doi.org/10.1146/annurev-pathol-020712-164023.

[17] Wang J, Hossain M, Thanabalasuriar A, Gunzer M, Meininger C, Kubes P. Visualizing the function and fate of neutrophils in sterile injury and repair. Science 2017;358:111–6. https://doi.org/10.1126/science.aam9690.

[18] Das S, Maras JS, Hussain MS, Sharma S, David P, Sukriti S, et al. Hyperoxidized albumin modulates neutrophils to induce oxidative stress and inflammation in severe alcoholic hepatitis. Hepatology 2017;65:631–46. https://doi.org/10.1002/HEP.28897.

[19] Boussif A, Rolas L, Weiss E, Bouriche H, Moreau R, Périanin A. Impaired intracellular signaling, myeloperoxidase release and bactericidal activity of neutrophils from patients with alcoholic cirrhosis. J Hepatol 2016;64:1041–8. https://doi.org/10.1016/J.JHEP.2015.12.005.

[20] Moreau R, Jalan R, Gines P, Pavesi M, Angeli P, Cordoba J, et al. Acute-on-chronic liver failure is a distinct syndrome that develops in patients with acute decompensation of cirrhosis. Gastroenterology 2013;144:1426–37, 1437.e1-9.

https://doi.org/10.1053/J.GASTRO.2013.02.042.

[21] Hilscher MB, Sehrawat T, Arab JP, Zeng Z, Gao J, Liu M, et al. Mechanical Stretch Increases Expression of CXCL1 in Liver Sinusoidal Endothelial Cells to Recruit Neutrophils, Generate Sinusoidal Microthombi, and Promote Portal Hypertension. Gastroenterology 2019;157:193-209.e9. https://doi.org/10.1053/J.GASTRO.2019.03.013.

[22] Zhang R, Su L, Fu M, Wang Z, Tan L, Chen H, et al. CD177+ cells produce neutrophil extracellular traps that promote biliary atresia. J Hepatol 2022;77:1299–310. https://doi.org/10.1016/j.jhep.2022.06.015.

[23] Yang W, Tao Y, Wu Y, Zhao X, Ye W, Zhao D, et al. Neutrophils promote the development of reparative macrophages mediated by ROS to orchestrate liver repair. Nat Commun 2019;10:1–14. https://doi.org/10.1038/s41467-019-09046-8.

[24] Marwick JA, Mills R, Kay O, Michail K, Stephen J, Rossi AG, et al. Neutrophils induce macrophage anti-inflammatory reprogramming by suppressing NF-κB activation. Cell Death Dis 2018;9:665. https://doi.org/10.1038/s41419-018-0710-y.

[25] Altamirano J, Miquel R, Katoonizadeh A, Abraldes JG, Duarte-Rojo A, Louvet A, et al. A Histologic Scoring System for Prognosis of Patients With AlcoholicHepatitis. Gastroenterology 2014;146:1231. https://doi.org/10.1053/J.GASTRO.2014.01.018.

[26] Cho Y, Bukong TN, Tornai D, Babuta M, Vlachos IS, Kanata E, et al. Neutrophil extracellular traps contribute to liver damage and increase defective low-density neutrophils in alcoholic hepatitis. J Hepatol 2022;78:28–44. https://doi.org/10.1016/J.JHEP.2022.08.029.

[27] Pose E, Sancho-Bru P, Coll M. 3,5-Diethoxycarbonyl-1,4-Dihydrocollidine Diet: A Rodent Model in Cholestasis Research. Methods Mol Biol 2019;1981:249–57. https://doi.org/10.1007/978-1-4939-9420-5_16.

[28] Simon H-U. Neutrophil apoptosis pathways and their modifications in inflammation. Immunol Rev 2003;193:101–10. https://doi.org/10.1034/J.1600-065X.2003.00038.X.

[29] Salic A, Mitchison TJ. A chemical method for fast and sensitive detection of DNA synthesis in vivo. Proc Natl Acad Sci 2008;105:2415–20. https://doi.org/10.1073/PNAS.0712168105.

[30] Ballesteros I, Rubio-Ponce A, Genua M, Lusito E, Kwok I, Fernández-Calvo G, et al. Co-option of Neutrophil Fates by Tissue Environments. Cell 2020;183:1282-1297.e18. https://doi.org/10.1016/J.CELL.2020.10.003.

[31] Kim JH, Podstawka J, Lou Y, Li L, Lee EKS, Divangahi M, et al. Aged polymorphonuclear leukocytes cause fibrotic interstitial lung disease in the absence of regulation by B cells. Nat Immunol 2018;19:192–201. https://doi.org/10.1038/s41590-017-0030-x.

[32] Peng Z, Liu C, Victor AR, Cao D-Y, Veiras LC, Bernstein EA, et al. Tumors exploit CXCR4hiCD62Llo aged neutrophils to facilitate metastatic spread. Oncoimmunology 2021;10:1870811. https://doi.org/10.1080/2162402X.2020.1870811.

[33] Casanova-Acebes M, Pitaval C, Weiss LA, Nombela-Arrieta C, Chèvre R, A-González N, et al. Rhythmic modulation of the hematopoietic niche through neutrophil clearance. Cell 2013;153:1025. https://doi.org/10.1016/J.CELL.2013.04.040.

[34] Metzemaekers M, Gouwy M, Proost P. Neutrophil chemoattractant receptors in health and disease: double-edged swords. Cell Mol Immunol 2020;17:433–50. https://doi.org/10.1038/s41423-020-0412-0.

[35] Hartl D, Krauss-Etschmann S, Koller B, Hordijk PL, Kuijpers TW, Hoffmann F, et al. Infiltrated Neutrophils Acquire Novel Chemokine Receptor Expression and Chemokine Responsiveness in Chronic Inflammatory Lung Diseases. J Immunol 2008;181:8053–67. https://doi.org/10.4049/JIMMUNOL.181.11.8053.

[36] Mühleder S, Macarena Fernández-Chacón ·, Garcia-Gonzalez I, Benedito · Rui. Endothelial sprouting, proliferation, or senescence: tipping the balance from physiology to pathology. Cell Mol Life Sci 2021;78:1329–54. https://doi.org/10.1007/s00018-020-03664-y.

[37] Tang Y, Li H, Li J, Liu Y, Li Y, Zhou J, et al. Macrophage scavenger receptor 1 contributes to pathogenesis of fulminant hepatitis via neutrophil-mediated complement activation. J Hepatol 2018;68:733–43. https://doi.org/10.1016/J.JHEP.2017.11.010.

[38] Windt DJ van der, Sud V, Zhang H, Varley PR, Goswami J, Yazdani HO, et al. Neutrophil extracellular traps promote inflammation and development of hepatocellular carcinoma in nonalcoholic steatohepatitis. Hepatology 2018;68:1347–60. https://doi.org/10.1002/HEP.29914.

[39] Bukong TN, Cho Y, Iracheta-Vellve A, Saha B, Lowe P, Adejumo A, et al. Abnormal neutrophil traps and impaired efferocytosis contribute to liver injury and sepsis severity after binge alcohol use. J Hepatol 2018;69:1145–54. https://doi.org/10.1016/J.JHEP.2018.07.005.

[40] Yang L, Liu Q, Zhang X, Liu X, Zhou B, Chen J, et al. DNA of neutrophil

615 extracellular traps promotes cancer metastasis via CCDC25. Nature
616 2020;583:133–8. https://doi.org/10.1038/s41586-020-2394-6.
617 [41] Xue R, Zhang Q, Cao Q, Kong R, Xiang X, Liu H, et al. Liver tumour
618 immune microenvironment subtypes and neutrophil heterogeneity. Nature
619 2022;612:141–7. https://doi.org/10.1038/S41586-022-05400-X.
620 [42] Makkar K, Tomer S, Rathi S, Arora SK, Taneja S, Duseja A, et al.
621 Neutrophil Dysfunction in Acute on Chronic Liver Failure. J Clin Exp
622 Hepatol 2017;7:S12–3. https://doi.org/10.1016/J.JCEH.2017.05.032.
623 [43] Huang H, Tohme S, Al-Khafaji AB, Tai S, Loughran P, Chen L, et al.
624 Damage-associated molecular pattern–activated neutrophil extracellular
625 trap exacerbates sterile inflammatory liver injury. Hepatology
626 2015;62:600–14. https://doi.org/10.1002/HEP.27841.
627 [44] Mattos MS, Lopes ME, Araujo AM de, Alvarenga DM, Nakagaki BN,
628 Mafra K, et al. Prolonged neutrophil survival at necrotic sites is a
629 fundamental feature for tissue recovery and resolution of hepatic
630 inflammation. J Leukoc Biol 2020;108:1199–213.
631 https://doi.org/10.1002/JLB.1MA0420-634R.
632 [45] Calvente CJ, Tameda M, Johnson CD, Pilar H del, Lin YC, Adronikou N,
633 et al. Neutrophils contribute to spontaneous resolution of liver
634 inflammation and fibrosis via microRNA-223. J Clin Invest
635 2019;129:4091–109. https://doi.org/10.1172/JCI122258.
636 [46] Saijou E, Enomoto Y, Matsuda M, Kok CY-Y, Akira S, Tanaka M, et al.
637 Neutrophils alleviate fibrosis in the CCl4-induced mouse chronic liver
638 injury model. Hepatol Commun 2018;2:703–17.
639 https://doi.org/10.1002/HEP4.1178.

[47] Albrengues J, Shields MA, Ng D, Park CG, Ambrico A, Poindexter ME, et al. Neutrophil extracellular traps produced during inflammation awaken dormant cancer cells in mice. Science 2018;361:eaao4227. https://doi.org/10.1126/SCIENCE.AAO4227.

FIGURE LEGENDS

Fig. 1. Ductular reaction associated neutrophils (DRANs) are recruited to the biliary epithelium. (A) Immunofluorescence of MPO and KRT7 in liver sections of patients with alcohol-related liver disease (ALD), non-alcoholic fatty liver disease (NASH), hepatitis C and B virus (HCV and HBV) and primary biliary cholangitis (PBC). Scale bar: 100μm. **(B)** Immunofluorescence of DRANs (MPO) at biliary epithelium (KRT7) in hepatic biopsies of ALD patients. Percentage of MPO+ cells at periportal areas and minimum distance of MPO+ cells to KRT7+ cells. Scale bar: 100μm. **(C)** Clearing of 3mm-liver section of a cirrhotic patient. Arrows show neutrophils (MPO) attached to biliary cells (KRT7). **(D)** SD-IVM images. **(E)** 3D-reconstruction of neutrophils recruited at biliary epithelium in 1-week DDC mouse. **(F)** Images of DDC mice liver sections stained for Ly6G and EPCAM. All data is presented as mean ± SEM. *p<0.05, **p<0.01, ***p<0.001 as determined by One-way ANOVA with Tukey's multiple comparison test (B, F).

Fig. 2. DRANs are immobilized at the biliary epithelium and remain static. (A) Time-lapse SD-IVM images. **(B)** SD-IVM images of focal thermal injury (FTI) (Sytox Green) in 1-week DDC mice. Quantification of neutrophils retained at $EpCAM^+$ cells per field of view (FOV). **(C)** Flow cytometry plots showing $Ly6G^+$ EdU^+ neutrophils. **(D)** Percentage of $Ly6G^+$ EdU^+ neutrophils (n=3-4 mice per time point). Data presented as mean ± SEM. Each time point was compared by Two-way ANOVA with Dunnett's multiple comparison test versus day 3 (bone marrow samples) or day 4 (liver and blood samples). *p<0.05, **p<0.01 and ***p<0.001. **(E)** Immunofluorescence (scale bar: 50μm) and EdU immunohistochemistry (scale bar: 100μm) of liver sections of mice fed with DDC after 5 days of EdU injection.

Fig. 3. Liver neutrophils in chronic liver damage acquire an aged and pro-inflammatory phenotype. Flow cytometry analysis of the expression of CXCR4 **(A)** and L-selectin **(B)** in $Ly6G^+$ cells (n= 3 mice per group). **(C)** Flow cytometry analysis of DDC liver neutrophils (n=3 mice per group). **(D)** Flow cytometry analysis of liver neutrophils (n=5 mice per group). **(E)** Principal component analysis (PCA) of neutrophils transcriptomic data (n=3 mice per group). **(F)** Enriched gene ontology (GO) biological processes in liver neutrophils compared to blood neutrophils. **(G)** Heat map of differentially expressed inflammatory cytokines and receptors (n=3 mice per group). **(H)** Flow cytometry analysis of CCR2 expression in $Ly6G^+$ neutrophils in DDC-fed mice (n=3 mice per group). **(I)** Heat map of differentially expressed genes associated to significantly enriched GO annotations (n=3 mice per group). All data is presented as mean ± SEM. *p<0.05, **p<0.01 and ***p<0.001 as determined by One-way ANOVA with Tukey's multiple comparison test (A, B) and Student's t-test (C, D, H).

Fig. 4. Liver neutrophils in chronic injury present an altered functionality. **(A)** Gene expression analysis of liver and circulating neutrophils from DDC mice (n=4 mice per group). **(B)** Supernatant levels of cultured neutrophils stimulated with LPS (100ng/mL) or vehicle for 6 hours (n=4 mice per group). **(C)** Phagocytic activity of neutrophils isolated from DDC and control mice (n=5 mice per group). Phagocytic index: % of $Ly6G^+$E. coli-$FITC^+$ cells x MIF/100. **(D)** Neutrophil oxidative burst at basal or PMA-stimulated contexts in neutrophils from DDC and control mice (n=5-6 mice per group). Burst index: % of $Ly6G^+$ $Rhodamine^+$ cells x MIF/100. **(E)** Images and number of migrated neutrophils (n=3) when exposed to biliary organoid CM (n=3) and SCH-527123 for 2 hours (50μM). Scale bar: 100μm **(F)** Gene expression analysis of neutrophils (n=3) treated with organoid conditioned medium (CM) (n=3) and SCH-527123 (50μM) for 6 hours. **(G)** Flow cytometry analysis of CCR2, L-selectin, CD11b and CXCR4 expression in neutrophils (n=4-5) treated for 18 hours with organoid CM (n=3) and SCH-527123 (50μM). All data is presented as mean ± SEM. *p<0.05, **p<0.01 and ***p<0.001 as determined by Two-way ANOVA with Sidak's multiple comparison (A), One-way ANOVA with Tukey's multiple comparison (*Cxcl1* and *Il1b* in E, F, CCR2, CD11b and CXCR4 in G), Kruskal-Wallis test with Dunn's multiple comparison (B, *Tnf* and *Il6* in E; L-selectin in G) or Student's t-test (C, D).

Fig. 5. Long-term depletion of neutrophils in chronic liver injury leads to a decrease in proliferating biliary epithelial cells. (A) Immunohistochemistry analysis of livers of control and DDC mice treated with anti-Ly6G antibody (1A8) or isotype (n=4 mice per group). Scale bars: 100μm. **(B)** Staining of progenitor markers in mice treated with anti-Ly6G antibody (1A8) and isotype. Scale bars: 100μm. **(C)** Immunofluorescence of KRT19 and Cyclin D1 (CCND1) of liver sections of mice treated with anti-Ly6G antibody (1A8) and isotype (n=3 mice per group). Scale bars: 50μm. All data is presented as mean ± SEM. *p<0.05, **p<0.01 and ***p<0.001 as determined by One-way ANOVA with Tukey's multiple comparison test (MPO, KRT19, S/R in A), One-way ANOVA Kruskal-Wallis with Dunn's multiple comparison test (CD31 in A) and Mann-Whitney test (C).

Fig. 6. Blocking neutrophil recruitment by CXCR1/2 inhibitor reduces biliary epithelium expansion in chronic injury. (A) Mice were fed with DDC and daily treated with CXCR1/2 inhibitor (SCH-527123) for 3 weeks at a dose of 50mg/kg. **(B)** Immunohistochemistry analysis of liver sections of control and 3-weeks DDC-fed mice treated with SCH-527123 or vehicle (n=5-6 mice per group). Scale bars: 100μm. **(C)** Progenitor markers immunofluorescence in liver sections of mice fed with DDC for 3 weeks and treated with SCH-527123 inhibitor or vehicle. Scale bars: 100μm. **(D)** Immunofluorescence of KRT19 and CCND1 in mice treated with SCH-527123 or vehicle (n=3-5 mice per group). Scale bars: 50μm. Data presented as mean ± SEM. *p<0.05, **p<0.01 and ***p<0.001 as determined by One-way ANOVA with Tukey's multiple comparison test (A) and Student's t-test (D).

Fig. 7. Depletion of NETosis and elastase release reduces liver progenitor cell expansion. (A) Immunofluorescence of MPO and citrullinated histone H3 (citH3) in WT and PAD4$^{-/-}$ liver sections (n=4 mice per group). Scale bars: 100μm. **(B)** Immunohistochemistry analysis of WT and PAD4$^{-/-}$ mice liver sections (n=4-7 mice per group). Scale bars: 100μm. **(C)** Progenitor markers immunofluorescence of KRT19-EpCAM and KRT19-SOX9 in WT and PAD4$^{-/-}$ mice liver sections. Scale bars: 100μm. **(D)** Immunofluorescence of KRT19 and

Cyclin D1 (CCND1) in WT and PAD4$^{-/-}$ mice (n=4-6 mice per group). Scale bars: 50µm. **(E)** Immunofluorescence of NETs in WT and NE$^{-/-}$ liver sections (n=4 mice per group). Scale bars: 100µm. **(F)** Immunohistochemistry analysis of MPO and KRT19 in WT and NE$^{-/-}$ mice liver sections (n=4-5 mice per group). Scale bars: 100µm. **(G)** Progenitor markers immunofluorescence in WT and NE$^{-/-}$ mice liver sections. Scale bars: 100µm. **(H)** Immunofluorescence of KRT19 and CCND1 in WT and NE$^{-/-}$ mice. Scale bars: 50µm. **(I)** Images of biliary organoids and WT or NE$^{-/-}$ neutrophils co-culture. Organoid area is normalized per microcavity area. Each measurement represents a technical replicate consisting of the average area of at least 40 microcavities (n=3 mice-derived organoids). Scale bar: 500µm. Data presented as mean ± SEM. *p<0.05, **p<0.01 and ***p<0.001 as determined by Student's t-test (A, B, D, E, F, H) and One-way ANOVA with Tukey's multiple comparison test (I)**.**

Figure 1

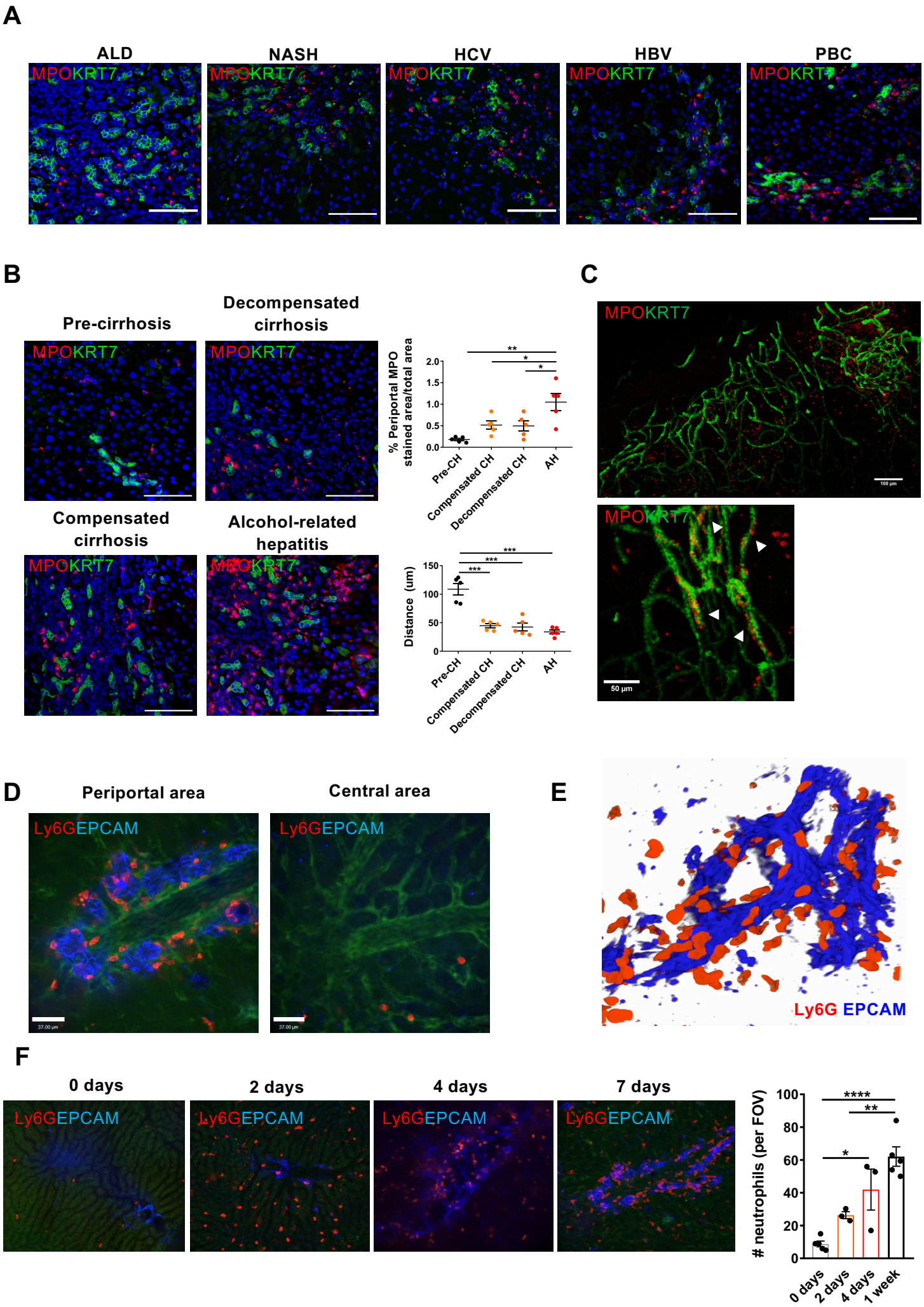
A
ALD
NASH
HCV
HBV
PBC
MPOKRT7
B
Pre-cirrhosis
Decompensated cirrhosis
Compensated cirrhosis
Alcohol-related hepatitis
% Periportal MPO stained area/total area
Distance (um)
Pre-CH
Compensated CH
Decompensated CH
AH
C
100 µm
50 µm
D
Periportal area
Central area
Ly6GEPCAM
E
Ly6G EPCAM
F
0 days
2 days
4 days
7 days
neutrophils (per FOV)
1 week

Figure 2

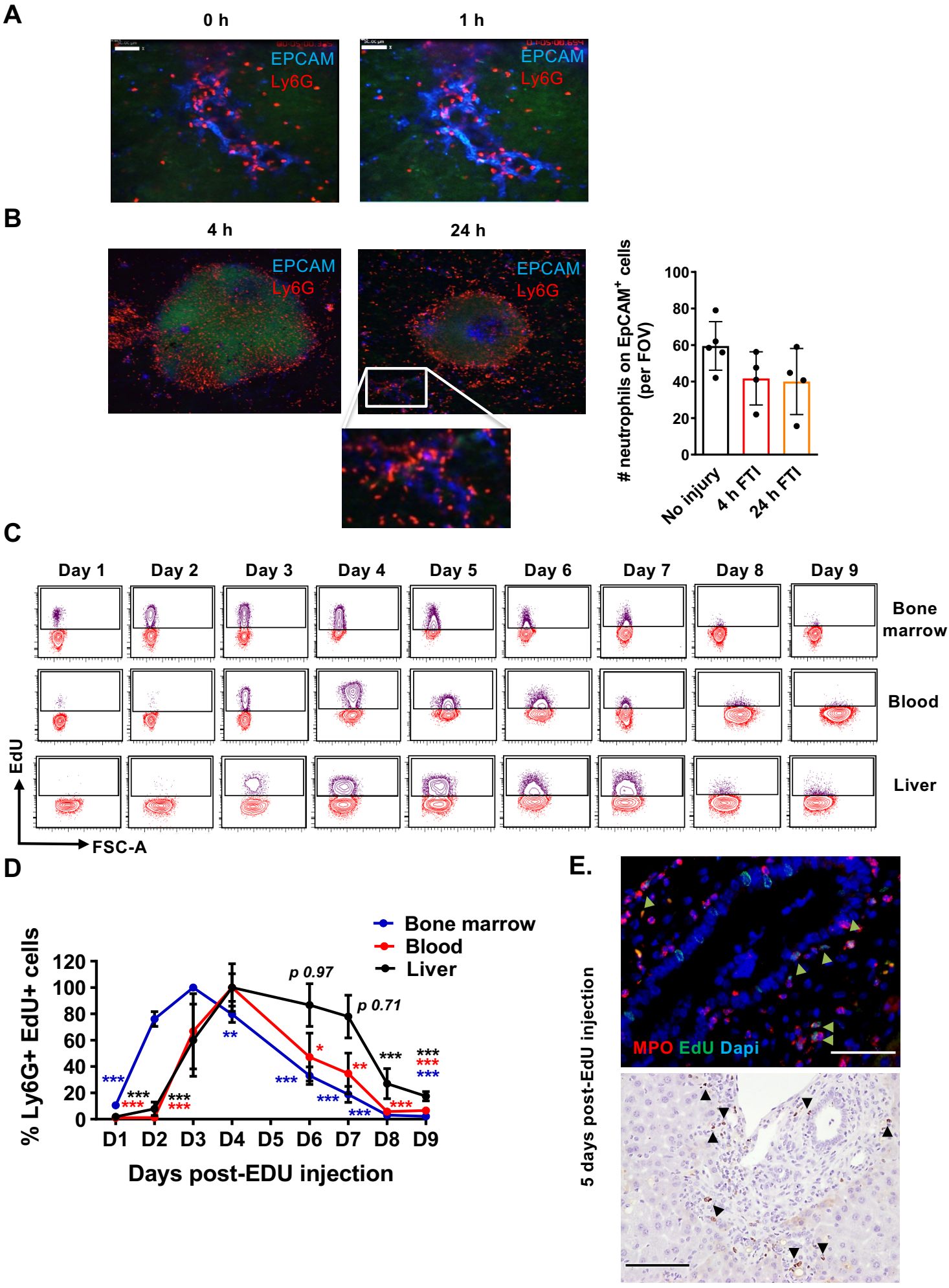
A
0 h
1 h
EPCAM
Ly6G
B
4 h
24 h
EPCAM
Ly6G
neutrophils on EpCAM+ cells (per FOV)
100
80
60
40
20
0
No injury
4 h FTI
24 h FTI
C
Day 1
Day 2
Day 3
Day 4
Day 5
Day 6
Day 7
Day 8
Day 9
Bone marrow
Blood
Liver
EdU
FSC-A
D
Bone marrow
Blood
Liver
% Ly6G+ EdU+ cells
120
100
80
60
40
20
0
p 0.97
p 0.71
D1
D2
D3
D4
D5
D6
D7
D8
D9
Days post-EDU injection
E.
MPO EdU Dapi
5 days post-EdU injection

Figure 3

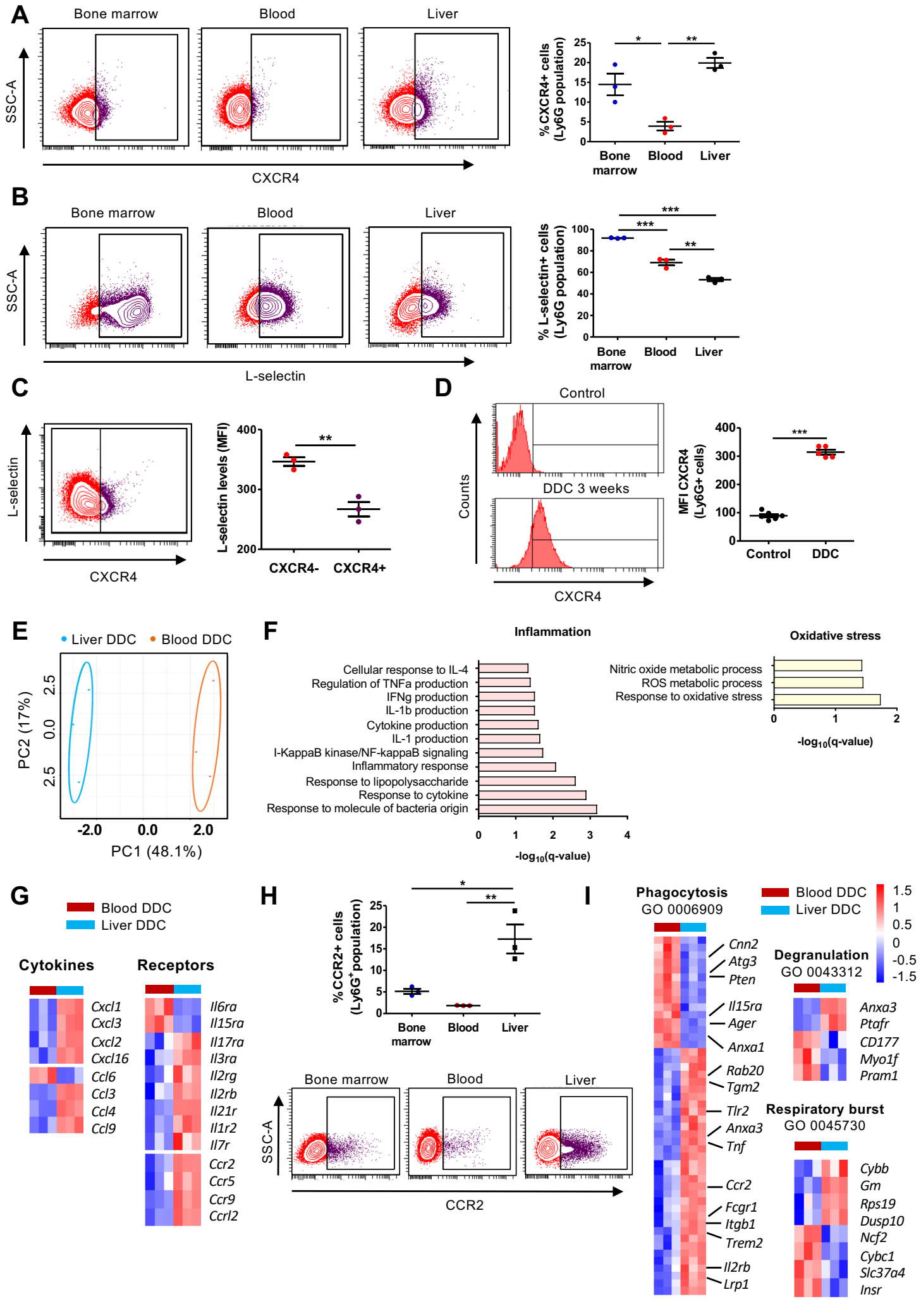
A
Bone marrow
Blood
Liver
SSC-A
CXCR4
% CXCR4+ cells (Ly6G population)
Bone marrow
Blood
Liver
B
Bone marrow
Blood
Liver
SSC-A
L-selectin
% L-selectin+ cells (Ly6G population)
Bone marrow
Blood
Liver
C
L-selectin
CXCR4
L-selectin levels (MFI)
CXCR4-
CXCR4+
D
Control
DDC 3 weeks
Counts
CXCR4
MFI CXCR4 (Ly6G+ cells)
Control
DDC
E
Liver DDC
Blood DDC
PC2 (17%)
PC1 (48.1%)
F
Inflammation
Cellular response to IL-4
Regulation of TNFa production
IFNg production
IL-1b production
Cytokine production
IL-1 production
I-KappaB kinase/NF-kappaB signaling
Inflammatory response
Response to lipopolysaccharide
Response to cytokine
Response to molecule of bacteria origin
-log10(q-value)
Oxidative stress
Nitric oxide metabolic process
ROS metabolic process
Response to oxidative stress
-log10(q-value)
G
Blood DDC
Liver DDC
Cytokines
Cxcl1
Cxcl3
Cxcl2
Cxcl16
Ccl6
Ccl3
Ccl4
Ccl9
Receptors
Il6ra
Il15ra
Il17ra
Il3ra
Il2rg
Il2rb
Il21r
Il1r2
Il7r
Ccr2
Ccr5
Ccr9
Ccrl2
H
% CCR2+ cells (Ly6G+ population)
Bone marrow
Blood
Liver
Bone marrow
Blood
Liver
SSC-A
CCR2
I
Phagocytosis
GO 0006909
Blood DDC
Liver DDC
Cnn2
Atg3
Pten
Il15ra
Ager
Anxa1
Rab20
Tgm2
Tlr2
Anxa3
Tnf
Ccr2
Fcgr1
Itgb1
Trem2
Il2rb
Lrp1
Degranulation
GO 0043312
Anxa3
Ptafr
CD177
Myo1f
Pram1
Respiratory burst
GO 0045730
Cybb
Gm
Rps19
Dusp10
Ncf2
Cybc1
Slc37a4
Insr

Figure 4

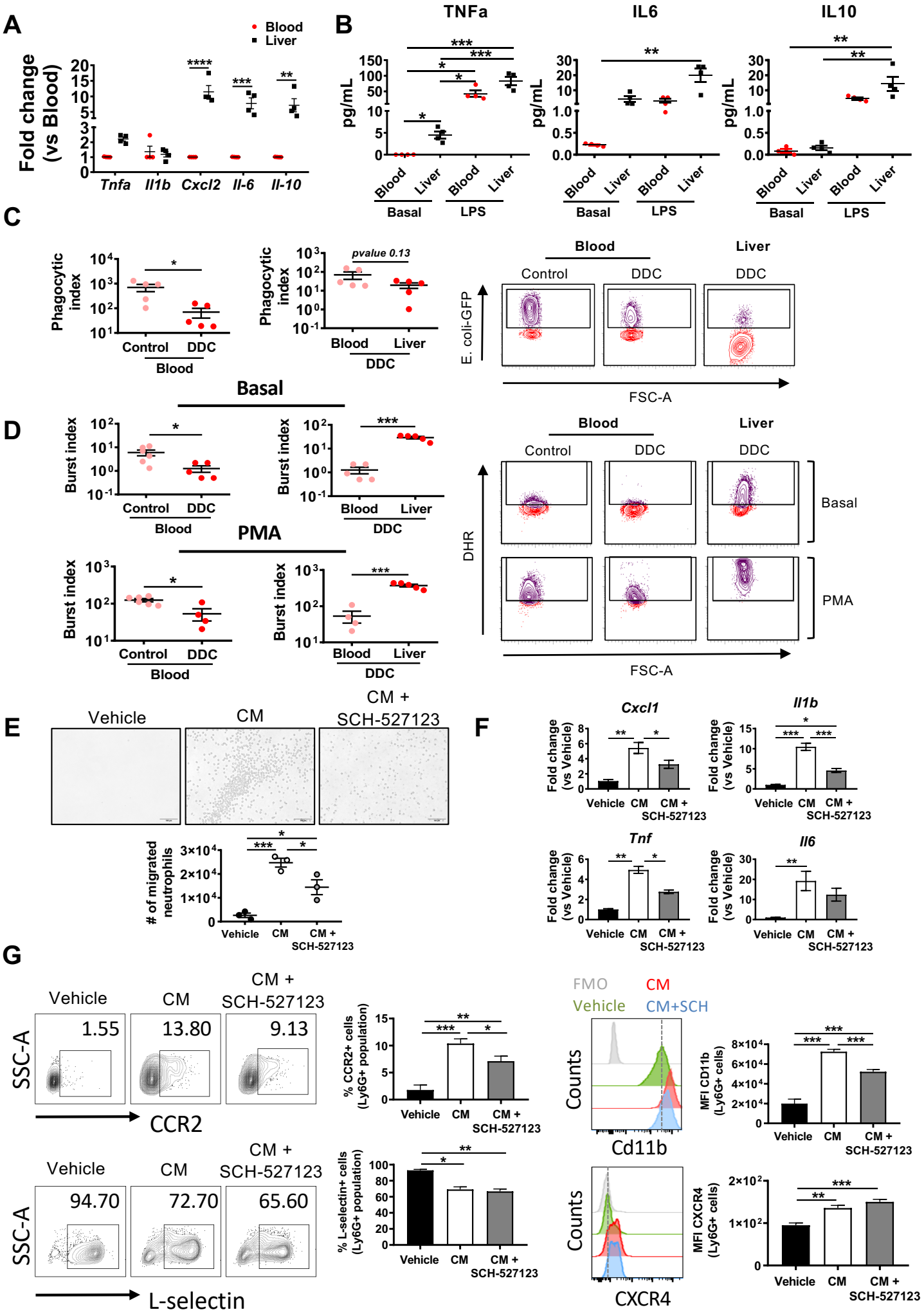
A
Blood
Liver
Fold change (vs Blood)
Tnfa
Il1b
Cxcl2
Il-6
Il-10
B
TNFa
IL6
IL10
pg/mL
Blood
Liver
Basal
LPS
C
Phagocytic index
Control
DDC
Blood
pvalue 0.13
Liver
E. coli-GFP
FSC-A
Basal
D
Burst index
PMA
DHR
E
Vehicle
CM
CM + SCH-527123
# of migrated neutrophils
F
Cxcl1
Il1b
Tnf
Il6
Fold change (vs Vehicle)
G
SSC-A
CCR2
1.55
13.80
9.13
% CCR2+ cells (Ly6G+ population)
L-selectin
94.70
72.70
65.60
% L-selectin+ cells (Ly6G+ population)
FMO
Vehicle
CM
CM+SCH
Counts
Cd11b
MFI CD11b (Ly6G+ cells)
CXCR4
MFI CXCR4 (Ly6G+ cells)

Figure 5

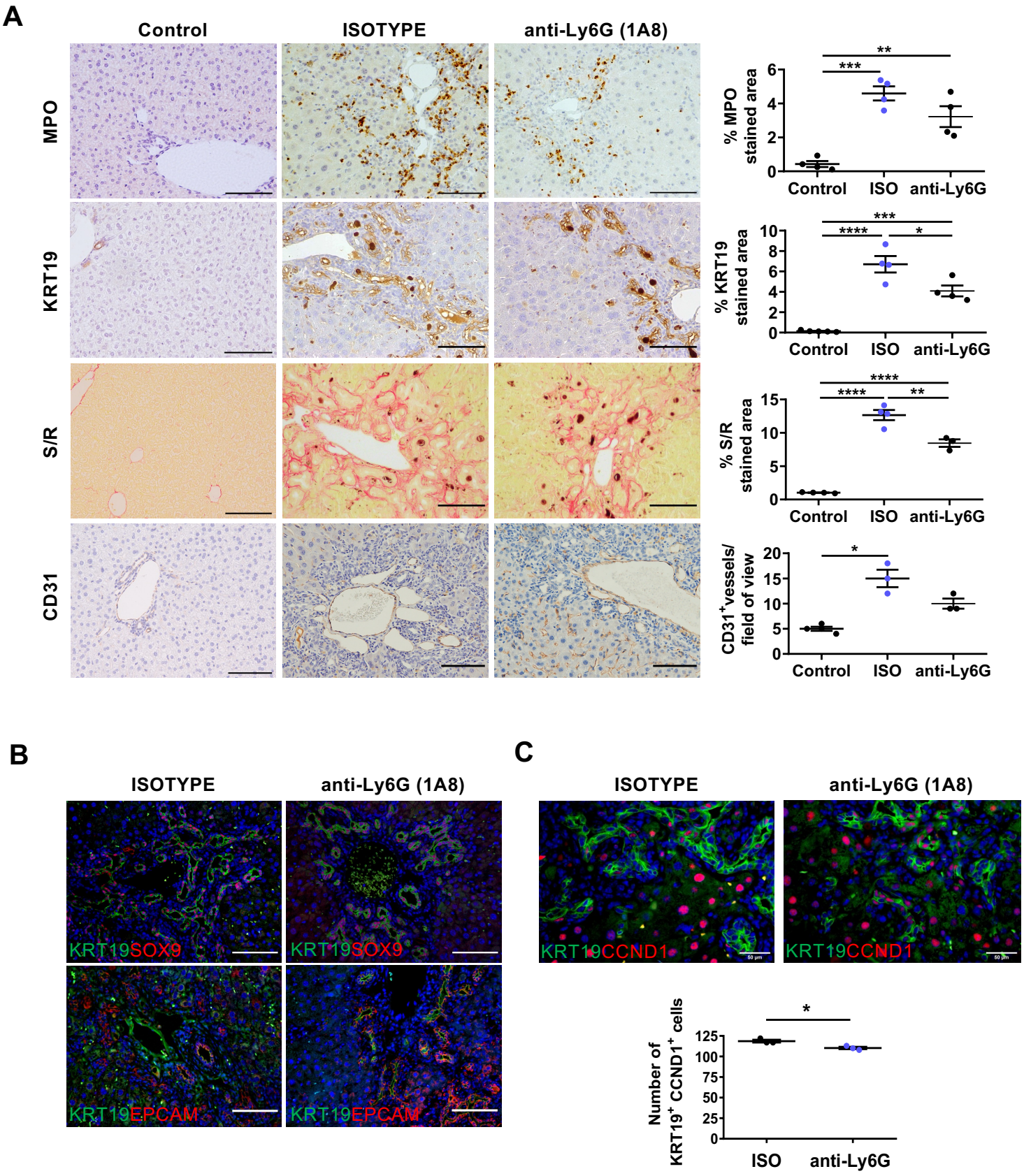
A
Control
ISOTYPE
anti-Ly6G (1A8)
MPO
KRT19
S/R
CD31
% MPO stained area
% KRT19 stained area
% S/R stained area
CD31+vessels/ field of view
Control
ISO
anti-Ly6G
B
ISOTYPE
anti-Ly6G (1A8)
KRT19SOX9
KRT19EPCAM
C
ISOTYPE
anti-Ly6G (1A8)
KRT19CCND1
Number of KRT19+ CCND1+ cells
ISO
anti-Ly6G

Figure 6

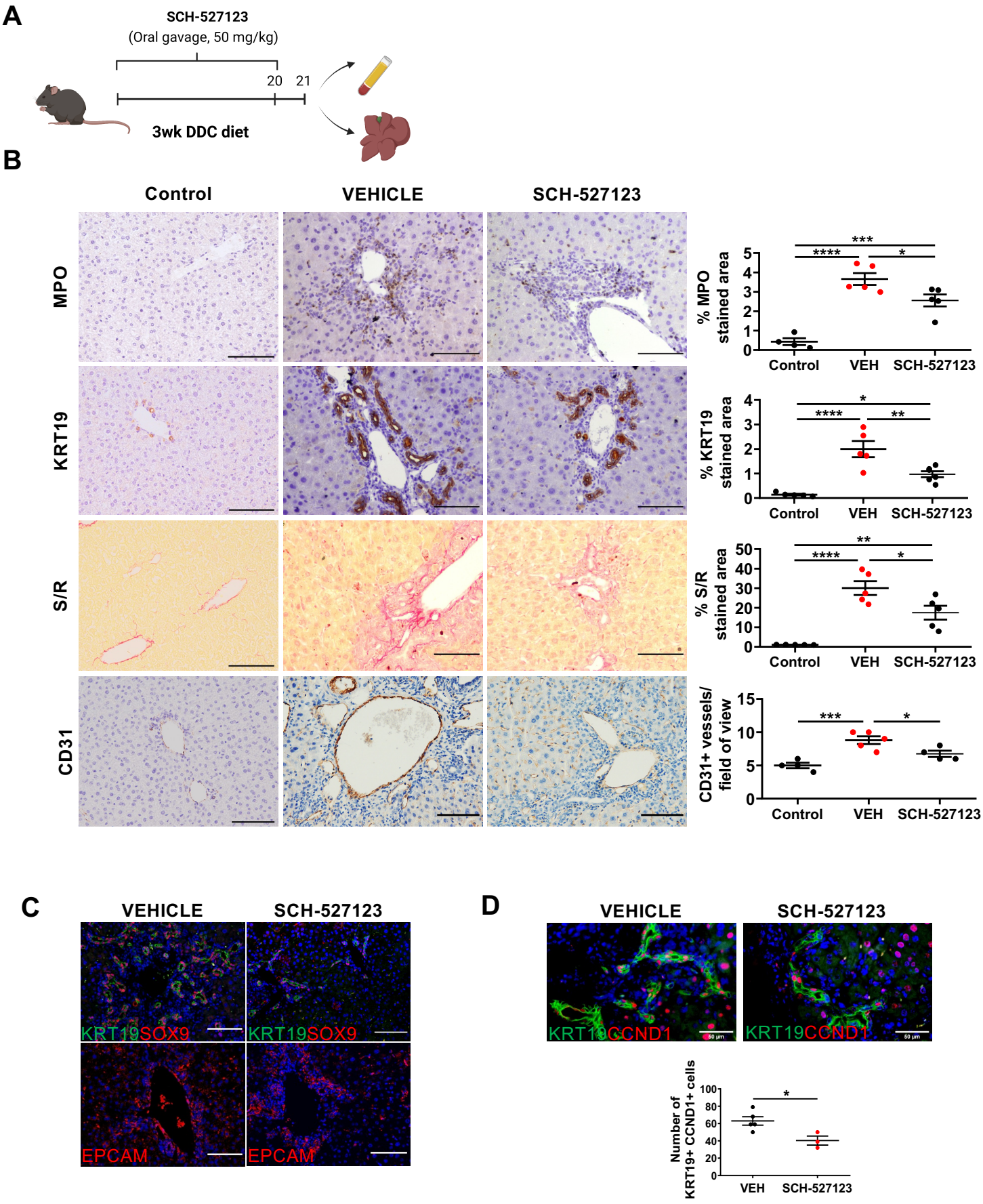
A
SCH-527123
(Oral gavage, 50 mg/kg)
20
21
3wk DDC diet
B
Control
VEHICLE
SCH-527123
MPO
KRT19
S/R
CD31
% MPO stained area
% KRT19 stained area
% S/R stained area
CD31+ vessels/ field of view
Control
VEH
SCH-527123
C
VEHICLE
SCH-527123
KRT19SOX9
EPCAM
D
VEHICLE
SCH-527123
KRT19CCND1
Number of KRT19+ CCND1+ cells
VEH
SCH-527123

Figure 7

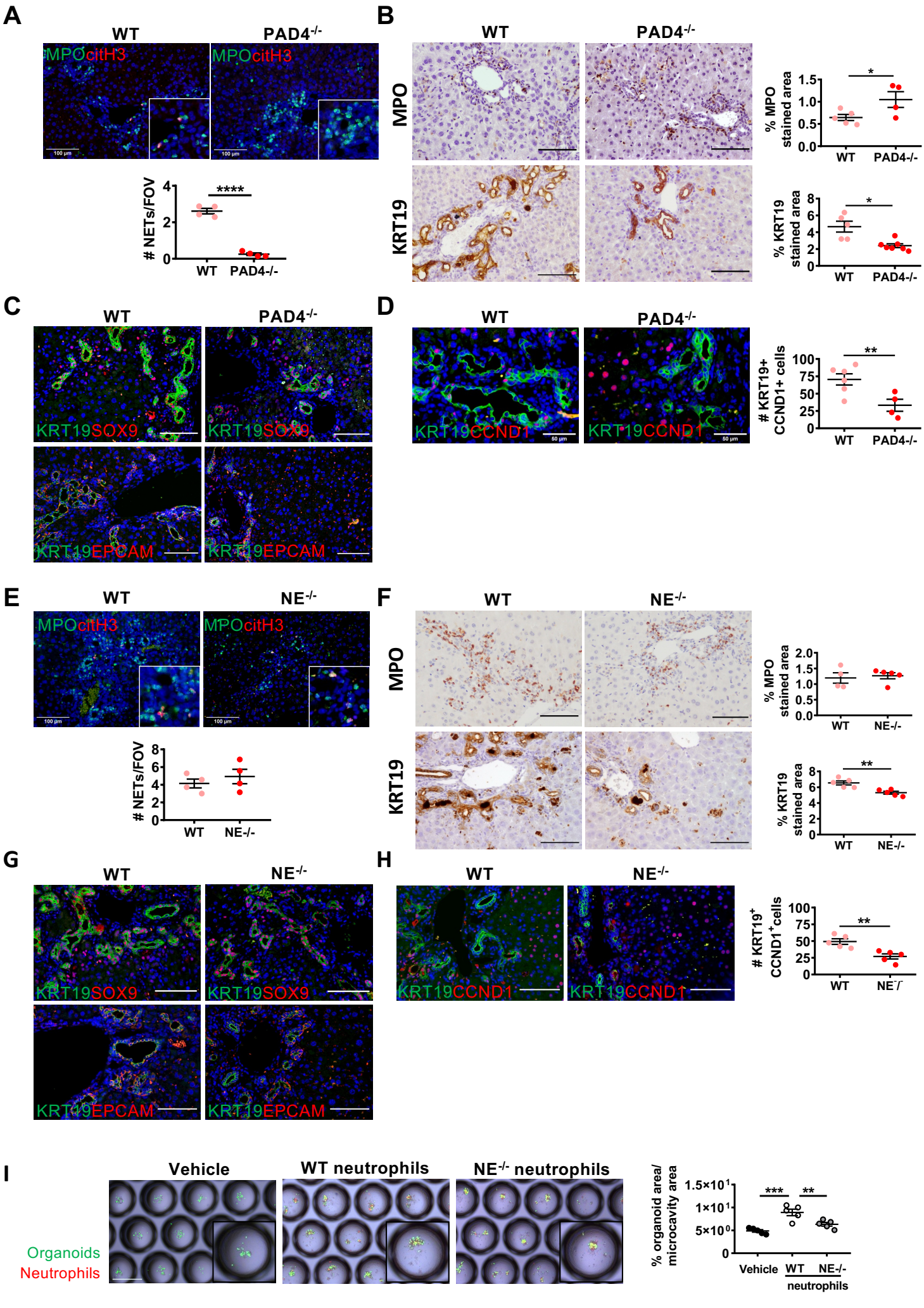
A
WT
PAD4-/-
MPOcitH3
NETs/FOV
****
WT
PAD4-/-
B
WT
PAD4-/-
MPO
KRT19
% MPO stained area
% KRT19 stained area
*
C
KRT19SOX9
KRT19EPCAM
D
KRT19CCND1
KRT19+ CCND1+ cells
**
E
NE-/-
F
G
H
KRT19+ CCND1+cells
I
Vehicle
WT neutrophils
NE-/- neutrophils
Organoids
Neutrophils
% organoid area/ microcavity area
***
Vehicle
neutrophils

Ductular reaction-associated neutrophils promote biliary epithelium proliferation in chronic liver disease

Silvia Ariño[1,3+], Beatriz Aguilar-Bravo[1+], Mar Coll[1,2,3+*], Woo-Yong Lee[4], *Moritz* Peiseler[4], Paula Cantallops[1], Laura Sererols-Viñas[1], Raquel A Martínez-García de la Torre[1], Celia Martínez-Sánchez[1,3], Jordi Pedragosa[1,7], Laura Zanatto[1], Jordi Gratacós-Ginès[1,5], Elisa Pose[1,2,3,5], Delia Blaya[1], Xènia Almodóvar[1], María Fernández-Fernández[1,6], Paloma Ruiz-Blázquez[1,6], Juan José Lozano[3], Silvia Affo[1,3], Anna M Planas[1,7], Pere Ginès[1,3,5], Anna Moles[1,6], Paul Kubes[4¥] and Pau Sancho-Bru[1,2,3¥*].

Table of contents

Supplementary Material and Methods

Animal models

10-12-week-old male and female C57BL/6J mice (Charles River) were fed with a standard rodent chow diet containing 0.1% 3,5-diethoxycarbonyl-1,4-dihydro-collidin (DDC) (Sigma-Aldrich, St. Louis, MO). This model has been previously reported to mimic histological and pathophysiological characteristics of chronic liver diseases in humans [1]. After one week of DDC treatment, DDC-treated and control female and male animals were sacrificed and liver, blood and bone marrow samples were collected for further neutrophil phenotype and function characterization.

As a neutrophil depletion model, 12-week-old male mice were treated with anti-Ly6G clone 1A8 antibody (500µg) or isotype (500µg) (BioXcell) every 2 days and simultaneously fed with DDC for 3 weeks. First antibody or isotype administration was performed 2 days before starting with DDC diet.

To inhibit CXCR1/2 receptor activity, the inhibitor SCH-527123 (MedChemExpress) was used. SCH-527123 was suspended in 20% 2-Hydroxypropyl-beta-cyclodextrin (HPβCD) (Sigma Aldrich). SCH-527123 inhibitor or vehicle were daily administered to 12-week-old male mice by oral gavage at a dose of 50mg/kg body weight for 3 weeks together with DDC diet. After this time, animals were sacrificed, and liver and blood samples were collected.

Neutrophil elastase and protein arginine deiminase 4 deficient mice ($NE^{-/-}$ and $PAD4^{-/-}$) were obtained from Jackson Laboratory. 12-week-old $NE^{-/-}$ and $PAD4^{-/-}$ male mice were fed with DDC diet for 3 weeks.

As secondary injury mice models, carbon tetrachloride (CCl4) was injected every two days for four weeks in 12-week-old female and male mice. For the bile duct ligation model (BDL), the bile duct was ligated for 14 days in 8-10 weeks C57BL6/J males.

All animal experiments were approved by the Ethics Committee of Animal Experimentation of the University of Barcelona and were conducted in accordance with the National Institute of Health Guide for the Care and Use of Laboratory Animals.

Mouse serum biochemical assays

Blood from mice was collected in heparinized tubes and analyzed by the Biomedical Diagnostic Center of Hospital Clinic, Barcelona. Serological analysis included the determination of alanine aminotransferase (ALT), aspartate aminotransferase (AST), lactate dehydrogenase (LDH) and alkaline phosphatase (AP) levels.

Spinning disk intravital microscopy

Image acquisition was carried out with Olympus IX81 inverted microscope, associated with an Olympus focus drive and a monitorized stage (Applied scientific Instrumentation) and fitted with a monitored objective turret equipped with 4x/0.16 UPLANSAPO, 10x/0.40 UPLANSAPO, and 20x/0.70 UPLANSAPO objective lenses and linked to a confocal light path (WaveFX; Quorum Technologies™). Briefly, mice were anesthetized with Ketamine and xylazine (200mg/kg and 10mg/kg, respectively). Next, the animals were catheterized through the tail vein and after abdominal surgery, the liver was appropriately exposed. Mice were intravenously injected with 4µL αEpCAM-APC

(eBioscience™) and 4µL αLy6G-PE (eBioscience™) monoclonal antibodies (0.5mg/mL) 4 hours prior SD-IVM. Velocity software (Perkin Elmer) was used to drive the confocal microscope. Acquired images were analyzed or exported as TIF images using Velocity software. Exported images were analyzed by ImageJ.

Human liver tissue clearing immunofluorescence

Liver tissue clearing and immunofluorescence from cirrhotic patients was performed following iDISCO protocol [2] with minor modifications. Briefly, liver tissue samples around 1mm thick were fixed in 4% paraformaldehyde at 4ºC overnight with shaking. Then, samples were washed three times in DPBS-/- with shaking at room temperature for 30 minutes. Samples were then dehydrated with methanol/water series and further bleached with 5% peroxide hydrogen in methanol overnight at 4ºC. Samples were then rehydrated with methanol/water series, washed and permeabilized at 37ºC for 2 days. After incubation in blocking solution for additional 2 days at 37ºC, samples were incubated with primary antibodies KRT7 (1:50, DAKO, M7018) and MPO (1:50, Abcam, ab9535) for 5 days at 37ºC. After one day of serial washes, secondary antibodies donkey anti-rabbit Cy3 (1:500, Jackson ImmunoResearch, 711-165-152), donkey anti-rat Alexa Fluor 488 (1:200, Jackson ImmunoResearch, 712-005-153), donkey anti-goat Alexa Fluor 488 (1:200, Jackson ImmunoResearch, 705-545-003), donkey anti-rabbit Alexa Fluor 488 (1:200, Jackson ImmunoResearch, 711-545-152) and goat anti-mouse Alexa Fluor 488 (1:200, Invitrogen, A11001) were added for 4 days at 37ºC. Samples were washed throughout a day, dehydrated with methanol/water series and incubated in 66% and 100% DCM (Sigma 270997-12) solutions for 3 hours and 15 minutes. Finally, after incubation with DiBenzyl Ether

(DBE, Sigma 108014), sample images were acquired with Confocal LSM880 Zeiss Microscope using Imaris Cell Software.

Neutrophil isolation

Liver samples were mashed through a 70µm cell strainer and digested with collagenase solution containing 50 mg/mL of collagenase A (Sigma-Aldrich, 37170821) and 0.01 mg/mL of DNaseI (Sigma-Aldrich, 10104159001) for 30 minutes at 37ºC. Digested samples were centrifuged at 50g for 3 minutes without break to precipitate hepatocytes. Supernatants were collected and pelleted. Pellets were suspended in 8 mL of 40% percoll solution and layered onto 3 mL of 70% percoll. After 30minutes centrifuge at 800g without break, the cell layer containing granulocytes was collected and washed twice with DPBS-/-.

Blood samples were washed with 2ml of FACS buffer (2% heat-inactivated FBS, 1% sodium azide in DPBS-/-) at 1500rpm for 5 minutes. Erythrocytes were lysed with Lysing Buffer (BD PharmaLyse) for 10 minutes at 37ºC.

Neutrophil isolation from bone marrow was performed as previously described [3]. Femurs and tibias were cut out and muscles removed. Bones were placed in a petri dish with HBSS-/- supplemented with 0.5% inactivated FBS (HBSS-prep). The ends of the bones were cut, and bone marrow was flushed into a 50 mL conical tube with a 25G needle and a 10 mL syringe filled with HBSS-prep. Suspension was pelleted at 400g for 5 minutes and resuspended in 10 mL of 0.2% NaCl for 30-40 seconds to lyse. Osmolarity was restored with 10 mL of 1.6% NaCl and filtered through a 70µm cell strainer. Lysed suspension was resuspended in 5 mL of HBSS-prep layered over 62.5% of percoll in HBSS-/- and

centrifuged at 1000g for 30 minutes without break. A cloudy pellet containing neutrophils was collected after centrifugation.

Collected cells from each organ were then used for flow cytometry analysis or immunomagnetic isolation.

RNA Sequencing of liver and blood neutrophils

Liver and circulating neutrophils from 1-week DDC-treated mice and liver neutrophils from control mice (n=3 mice per group) were isolated by Ly6G-immunomagnetic separation (Anti-Ly-6G MicroBeads UltraPure kit, Miltenyi Biotec, Gladbach, Germany) after liver suspension percoll gradient and blood lysis. RNA was isolated using the commercial kit RNeasy Micro Kit (Qiagen) following manufacturer's instructions. The quantity and quality of the RNAs were evaluated using Nanodrop and Agilent RNA 6000 Pico Chips (Agilent Technologies, Cat.# 5067-1513). Sequencing libraries were prepared using "SMARTer Stranded Total RNA-seq Kit v2 – Pico Input Mammalian" kit (Takara Bio USA, Cat.# 634411), following "SMARTer Stranded Total RNA-seq Kit v2 – Pico Input Mammalian User Manual (Rev. 063017)". Paired-ended sequencing was performed on Illumina platform. STAR program [4] against Rattus norvegicus genome (Rn6.0) was used for mapping the reads followed by the quantification of genes with the RSEM [5] program using Ensembl reference annotation v-91. After excluding genes with at least an expected value greater than ten, we used TMM method and limma-voom transformation [6] to normalize the non-biological variability. Differential expression between different groups was assessed using moderated t-statistics [7]. Principal component Analysis plots, Gene Ontology analysis and normalized expression heatmaps were built using R statistics software. Protein-protein interaction network from top 50 differentially expressed

genes ($p<0.05$) in circulating versus intrahepatic neutrophils was generated by string-db.org platform. Disconnected nodes and networks were removed. Resulting genes were analysed using the pathway analysis option from string-db.org.

Immunohistochemistry and immunofluorescence analysis

Paraffin embedded liver sections (3 µm) were stained for KRT7 (1:50, Dako, M701801), KRT19 (1:100, TROMA III, AB_2133570), SOX9 (1:500, Millipore, ab5535), EpCAM (1:200, Abcam, ab71916), CCND1 (1:100, Abcam, ab134175), CD31 (1:50, Abcam, ab28364), KI67 (1:50, abcam, ab16667), KRT7 (1:500, Thermofisher, 15539-1-AP), cleaved Caspase 3 (1:100, Cell signaling, 9661S), MPO (1:100, RyD, AF3667), P21 (1:5, HUGO 291, CNIO), S100A8/9 (1:100, Abcam, Ab22506), CD177 (1:50, Abcam, Ab203025), KI67 (1:50, Thermofisher, 14-5698-82), Ly6G (1:500, Biolegend, 127602), citrullinated histone H3 (1:1000, Abcam, Ab5103) and MPO (1:50, Abcam, ab9535).

Sections were deparaffinized and incubated in Target Retrieval Solution (Citrate Ph6, DAKO, Glostrup, Denmark), heated in a pressure cooker for 20 minutes, or rehydrated and antigen retrieved with EnVision Flex Target Retrieval Solution Low or High PH in a DAKO PT Link. Samples were incubated with primary antibody overnight at 4ºC. After washing in PBS, sections were incubated with secondary antibody and Diaminobenzidine (DAB, Dako) was used as a chromogen. Sections were then counterstained with hematoxylin.

For immunofluorescence staining, secondary antibodies donkey anti-rabbit Cy3 (1:500, Jackson ImmunoResearch, 111-165-003), donkey anti-rat Alexa Fluor 488 (1:200, Jackson ImmunoResearch, 712-546-153) and goat anti-mouse Alexa

Fluor 488 (1:200, Invitrogen, A11001) were incubated for 30 minutes at room temperature and eventually, sections were mounted with Mounting Medium for Fluorescence with 4',6-diamidino-2-phenylindole (DAPI) (Vector Laboratories, Burlingame, CA) for nuclear staining.

For detection of liver fibrosis, Sirius red staining was performed. Liver sections (5 µm) were deparaffined and hydrated in distilled water. Afterward, sections were incubated in thiosemicarbazide 0.5% for 10 minutes prior to incubation for 1 hour in a 0.1% Sirius Red solution. Finally, sections were dehydrated in alcohol and mounted with DPX Mounting Medium. Stained area quantification was performed by taken 10-15 random images at 20x magnification. Subsequently, percentage of stained area versus total image area was quantified with ImageJ. The number of positive CD31 vessels, CCND1 positive nuclei, citH3 and Ly6G positive neutrophils per field of view were manually counted at 20x or 40x magnification images using Fiji. Minimum distance between neutrophils (MPO+) and biliary cells (KRT7+) were calculated using QuPath software.

Mouse biliary organoid culture and conditioned medium collection

Liver organoids were obtained from control and 1-week DDC-treated mice. Mouse biliary organoids were generated following the stablished protocol by Broutier et al. [8] with minor modifications. Organoids were cultured in the defined expansion biliary medium consisting of Advanced DMEM/F12 (Thermo Fisher Scientific) supplemented with 1% HEPES (Gibco), 1% GlutaMax (Gibco), 1% Pen-Strep, 1x N2 supplement and 1x B27 supplement (without vitamin A) from Gibco; 250ng/mL recombinant human RSPO1 50 ng/mL recombinant human HGF and 100 ng/ml recombinant human FGF10 from Preprotech; 50 ng/mL mouse EGF (RyD), 1,25mM N-acetylcysteine, 10nM human [Leu^{15}]-gastrin I, and

10mM Nicotinamide from Sigma and 10μM Rho Inhibitor γ-27632 (Axon Medchem). Medium was changed every 2 days and passaged every week as previously described [8]. When organoids reached 80-90% confluency, expansion biliary medium was replaced by basal medium consisting in Advanced DMEM/F12 (Thermo Fisher Scientific) supplemented with 1% HEPES (Gibco), 1% GlutaMax (Gibco), 1% Pen-Strep. After 18 hours, organoid conditioned medium was collected and centrifuged for debri removal before using in neutrophil *in vitro* assays. All organoid lines used in this study has been confirmed to be negative for mycoplasma.

Neutrophil and biliary organoid co-culture

Mouse liver organoids were digested using Tryple Express (Gibco) for 30 minutes at 37ºC and neutrophils from WT and $NE^{-/-}$ bone marrows were isolated as described in the Neutrophils Isolation methods section. Organoid cells were stained with Vybrant CFDA Cell Tracer (Thermofisher, V12883) and neutrophils were labelled with WGA-AF594 dye (Thermofisher, W11262) following manufacturer's protocol. Number of viable cells was counted and 65.000 organoid cells were mixed with 325.000 WT or $NE^{-/-}$ neutrophils (ratio 1:5) per condition. Mixed organoid-neutrophils conditions and control conditions (only organoids and only neutrophils) were stimulated with 50nM PMA (MedChemExpress) and plated in a 24-well ultralow-attachment microcavities plate (Corning). As a culture medium, 20% of organoid expansion medium diluted in organoid basal medium (Advanced DMEM/F12, 1% HEPES, 1% GlutaMax, 1% Pen-Strep) was used. WT and $NE^{-/-}$ bone marrow neutrophils and PMA were refreshed every 3 days. Organoid area after 7 days of co-culture was measured

in at least 40 microcavities per condition and percentage was obtained after normalizing organoid area per microcavity area.

Neutrophil migration assay

Circulating neutrophils were isolated from 1-week male and female DDC mice by Ly6G-immunomagnetic separation (Anti-Ly-6G MicroBeads UltraPure kit, Miltenyi Biotec, Gladbach, Germany) after blood lysis. 600uL of organoid conditioned medium or vehicle (organoid basal medium) were added to low-attachment 24 well-plate. 3.0 µm-pore transwells (CellQuart, #9323002) were placed on the top of the added medium and after pre-treatment of neutrophils with 50µM SCH-527123 (MedChemExpress) or vehicle for 45 minutes, 250.000 neutrophils per condition were added within the insert. Migration was allowed for 2 hours and migrated neutrophils were manually quantified using Neubauer Chamber and Trypan-blue dead cell exclusion.

***In vitro* stimulation of neutrophils with LPS and biliary organoid conditioned medium**

$Ly6G^+$ neutrophils were isolated from liver and blood samples from DDC mice (n=4 mice per group) using the Anti-Ly-6G MicroBeads UltraPure kit (Miltenyi Biotec, Gladbach, Germany) following the manufacturer's instructions. Enriched neutrophil bone marrow fraction was isolated by percoll gradient. 250.000 neutrophils were plated per well in a 48 well-plate. For LPS stimulation, liver and blood neutrophils were incubated with RPMI supplemented with LPS (100 ng/ml) or vehicle. After 6 hours, neutrophils for RNA extraction and supernatants were collected. For organoid conditioned medium and stimulation and CXCR1/2 inhibitor treatment, bone marrow neutrophils were pre-treated for 45 minutes with

50µM SCH-527123 (MedChemExpress) or vehicle. Then, neutrophils were centrifuged and vehicle or organoid conditioned medium with or without SCH-527123 (50µM) were added. After 6 hours, neutrophils were collected for RNA extraction or flow cytometry analysis.

Cytokine detection on cell culture supernatant

Interleukin (IL) IL-6, IL-10 and tumor necrosis factor alpha (TNFα) concentrations were determined in the supernatants of cultured neutrophils after LPS stimulation (250.000 neutrophils/condition) using a Milliplex® MAP Mouse high sensitivity Cytokine/Chemokine Detection Panel (a multiple immunoassay based on Luminex Technology) following the manufacturer's instructions (EMD Millipore, Germany).

RNA Isolation and mRNA Expression Analysis

Total RNA was extracted from total liver tissue of mice models using Trizol (Life Technologies, Carlsbad, CA) and from cultured neutrophils using the commercial kit miReasy Micro Kit (Qiagen) following manufacturer's instructions. Total RNA extracted underwent quality control by Bioanalyzer 2100 (Agilent Technologies, Santa Clara, CA). Gene expression quantification was accomplished using Taqman gene expression assay probe and- primers and Platinum SYBR Green qPCR SuperMix (Thermofisher, Ref. 11733046) and PrimeTime® qPCR Primers (IDT). Quantitative real-time PCR (qPCR) was performed with an ABI 7900 HT cycler (Life Technologies) and QuantStudio 7 Pro (Applied Biosystems). Expression values were calculated based on the ΔΔCt method. The results were expressed as $2^{\wedge-\Delta\Delta Ct}$.

Flow cytometry analysis for phenotypic characterization

Neutrophils from 1-week DDC-fed mice (n=3-6 mice per group) were isolated from liver and bone marrow using a percoll gradient whereas blood was only lysed for further processing. Prior to surface staining, isolated neutrophils were incubated with Mouse BD Fc Block™ (BD; #553141; 1:200) to block non-antigen-specific staining. Blocking was performed in a total volume of 50 uL of FACS buffer (2% heat-inactivated FBS, 1% sodium azide in DPBS-/-) for 10 minutes at 4ºC. Following, cells were stained for 30 minutes at 4ºC in a final volume of 100 uL with the following fluorescent antibodies: Rat anti-mouse Ly6G-FITC (BD; #551460; 1:100), rat anti-mouse CD62L (L-selectin)-PE (eBioscience™; #12-0621-82; 1:100), rat anti-mouse CD11b-Alexa Fluor 647® (BD; #557686; 1:100), rat anti-mouse CD192 (CCR2)-BUV395 (BD, #747972, 1:200) and rat anti-mouse CD184 (CXCR4)-eFluor 450 (eBioscience™; #48-9991-82; 1:100). Cells were then washed and fixed in 4% paraformaldehyde for 15 minutes at room temperature. Afterwards, cells were washed and resuspended in 200 uL of FACS buffer before acquisition. The samples were evaluated by flow cytometry using a LSR Fortessa (BD). Positive gating was performed using a fluorescence minus one (FMO) control for each surface staining and calculations of median intensity fluorescence (MIF) were based on Ly6G+ cells. Data were analysed using BD FACSDIVA™ Software (BD) and FlowJo v10.8.1 Software.

Phagocytic and oxidative respiratory burst assays

The phagocytic and oxidative burst capacity of blood granulocytes from control mice (n=5 mice per group) compared to blood and liver granulocytes from 1-week DDC mice (n=5 mice per group) were analysed using Phagotest™ (BD; #341060) and Phagoburst™ (BD; #341058) kits, respectively. A density of $1x10^6$ liver

granulocytes or 100uL of heparinized whole blood were used per tube. For phagocytosis measurement, 5uL of opsonized FITC-labelled E. coli were added per tube and samples were incubated on ice (control samples) or at 37°C (test samples) for 60 minutes. In the case of burst analysis, neutrophils were incubated with reconstituted DHR125 solution (1:10) at 37ºC for 5 minutes followed by an incubation with wash buffer (control samples) or 675nM phorbol 12-myristate 13-acetate (PMA) (test samples) for 30 minutes at 37ºC. After incubation, phagocytosis-related samples were placed on ice and quenching solution was added to discriminate between surface-bound and internalized bacteria fluorescence. Blood and liver granulocytes were stained with rat anti-mouse Ly6G-APC (BD; #560599; 1:100) and rat anti-mouse Ly6G-PE (BD; #551461; 1:100). Blood was further lysed and fixed. Finally, cells were resuspended in 10% heat inactivated FBS in RPMI containing DNA staining solution for flow cytometry analysis (FACS Canto II). Positive gating was performed based on control samples. Phagocytic and burst index measures: (% of DHR^+/FITC-E. $coli^+$ cells * MFI of DHR^+/FITC-E. $coli^+$ cells)/100. Data were analysed using BD FACSDIVA™ Software (BD).

EdU staining assay

To evaluate the retention time of liver neutrophils in response to 1 week of DDC diet injury, 5-ethynyl-2′-deoxyuridine (EdU) was injected intraperitoneally into mice (n=4 mice per time point) at 50mg/kg. After 1, 2, 3, 4, 5, 6, 7, 8 or 9 days of EdU injuection, all mice were sacrified. Neutrophils from BM, liver and peripheral blood were isolated by Ly6G-immunomagnetic separation and were stained for EdU following the manufacturer's protocol of Click-iT™ Plus EdU Flow Cytometry Assay Kit (Thermofisher; #C10646) with minor modifications. Briefly, cells were

resuspended in 1% BSA in DPBS-/- at 1x10⁷cells/mL. Cells were stained with rat anti-mouse Ly6G-FITC (BD; #551460; 1:100) for 30 min at 4ºC and washed. Following, cells were fixed and permeabilized and EdU was detected in a final volume of 600uL with a cocktail containing Alexa Fluor™ 350 picolyl azide (1:1000), copper protectant (1:5) and 1X Click-iT™ EdU buffer additive (1:10) in D-PBS. Finally, cells were washed, resuspended in 200uL of FACS buffer and analysed by flow cytometry (LSR Fortessa; BD). Neutrophils isolated a DDC-fed mouse without EdU injection were used as a negative control. Percentage of EdU^+ cells was determined based on $Ly6G^+$ cells. Data were analysed using BD FACSDIVA^{TM} Software (BD).

Statistical Analysis

Experimental data are presented as mean values ± SEM. All parameters analyzed followed normal distribution by Shapiro-Wilk test unless indicated in the figure legend. For normal distributed data, unpaired two-tailed t test was used when 2 groups were compared, and comparison of more than two datasets was done using one-way analysis of variance (ANOVA) with Turkey's post-test or two-way ANOVA with Dunnett's post-test. For non-normal distributed data, Mann-Whitney test was used when 2 groups were compared, Kruskal-Wallis with Dunn's post-test or two-way ANOVA with Sidak's post-test were used when more than two groups were compared. Statistical analyses were performed using GraphPad software.

Supplementary Figures

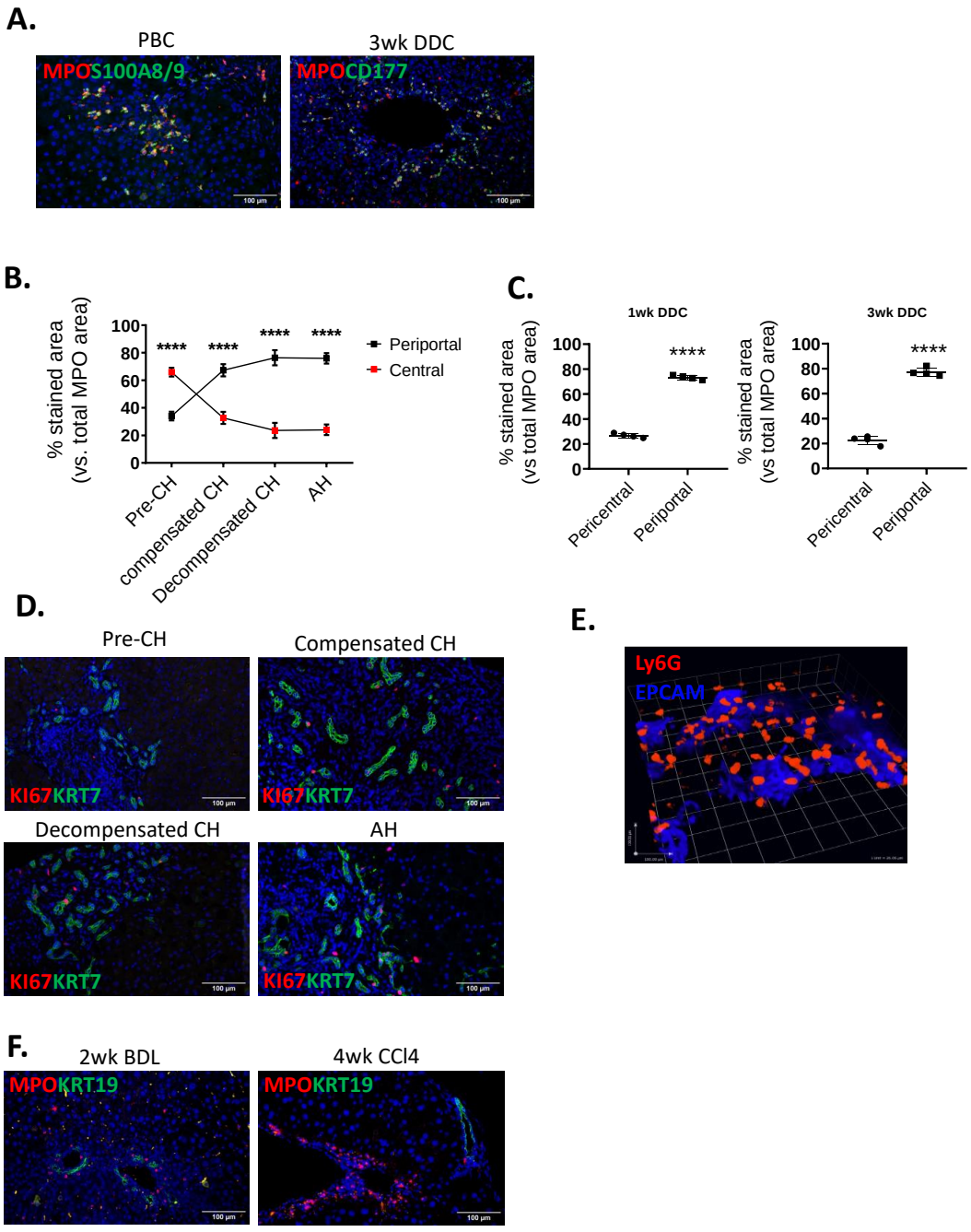

Supplementary Fig. 1. DRANs are recruited to biliary progenitor cells. **(A)** Representative images of neutrophils recruited to periportal areas co-stained for neutrophil markers MPO and S100A8/9 in human (primary biliary cholangitis, PBC) or MPO and CD177 in DDC-fed mice. **(B)** Percentage of periportal and central neutrophils throughout alcohol-related liver disease (ALD) progression: early (n=5), compensated cirrhosis (CH) (n=5), decompensated cirrhosis (n=5) and alcohol-related hepatitis (AH) (n=5). **(C)** Neutrophil quantification in pericentral and periportal (DRANs) areas in DDC-treated mice**. (D)**

Representative images of KI67 and KRT7 staining in ALD. Scale bar: 100 µm. **(E)** Representative intra-vital images showing DRANs (Ly6G, red) recruitment at DR cells (EpCAM, blue) in a mouse subjected to bile duct ligation for 5 days. **(F)** Representative immunofluorescence of neutrophil (MPO) distribution in relation to biliary cells (KRT7) in bile-duct ligation (BDL) and CCl4 liver injury mice models. Scale bars: 100 µm. Data presented as mean ± SEM. ****p<0.0001 as determined by Unpaired t-test.

A.

	Bone marrow				Blood				Liver			
	Absolute % EdU+ Ly6G+ cells	SEM	Normalized % EdU+ Ly6G+ cells	SEM	Absolute % EdU+ Ly6G+ cells	SEM	Normalized % EdU+ Ly6G+ cells	SEM	Absolute % EdU+ Ly6G+ cells	SEM	Normalized % EdU+ Ly6G+ cells	SEM
Day 1	5,267	0,994	10,523	1,986	0,450	0,210	1,010	0,472	0,625	0,217	1,832	0,637
Day 2	38,075	2,790	76,074	5,575	0,550	0,155	1,235	0,349	2,675	1,776	7,839	5,204
Day 3	**50,050**	0,811	**100,000**	1,620	39,633	11,362	66,723	28,634	20,473	9,365	59,993	27,444
Day 4	39,875	3,095	79,670	6,184	**44,550**	4,699	**100,000**	10,548	**34,125**	6,173	**100,000**	18,089
Day 6	16,525	3,333	33,017	6,660	21,000	8,104	47,138	18,191	29,575	5,551	86,667	16,268
Day 7	9,450	3,080	18,881	6,154	15,467	6,899	34,720	15,487	26,600	5,550	77,949	16,264
Day 8	1,550	1,022	3,097	2,042	2,575	1,120	5,780	2,514	9,225	3,926	27,033	11,506
Day 9	1,100	0,248	2,198	0,496	2,950	0,868	6,622	1,949	5,950	1,206	17,436	3,534

Supplementary Fig. 2. Liver neutrophils remain in the liver for 3.5 days before decaying. (A) Absolute percentage (%) of EdU+ Ly6G+ cells and normalized % of EdU+ Ly6G+ cells (versus the day of maximum percentage per organ) are shown for every day and for the bone marrow, blood and liver neutrophils. Maximum normalized % of cells and absolute % used for normalization are shown in bold. Data is presented as mean of 3-4 mice and SEM is shown.

A.

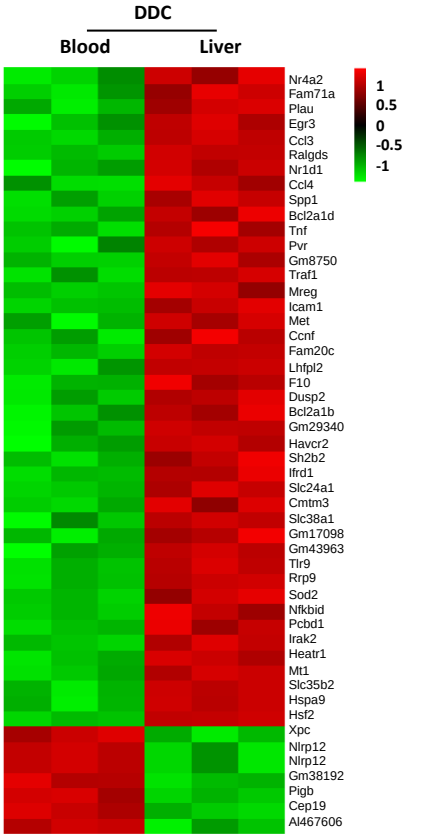

B.

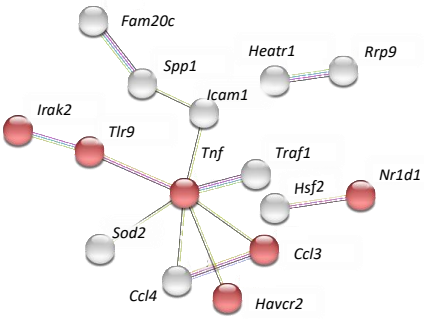

C.

	Gene ontology pathways	p. adjusted
GO:0030155	regulation of cell adhesion	1.99E-11
GO:0050900	leukocyte migration	3.44E-09
GO:0001819	positive regulation of cytokine production	1.72E-14
GO:0002237	response to molecule of bacterial origin	5.65E-13
GO:0032611	interleukin-1 beta production	2.44E-11
GO:0045321	leukocyte activation	2.78E-11
GO:0042110	T cell activation	3.44E-09
GO:0002224	toll-like receptor signaling pathway	3.52E-08
GO:0006909	phagocytosis	3.88E-08
GO:1903409	reactive oxygen species biosynthetic process	2.03E-07
GO:1903555	regulation of tnf superfamily cytokine production	2.99E-07
GO:0032635	interleukin-6 production	2.65E-06
GO:0045428	regulation of nitric oxide biosynthetic process	2.87E-06
GO:0048661	positive regulation of smooth muscle cell proliferation	3.06E-06
GO:1904018	positive regulation of vasculature development	6.27E-06
GO:0045766	positive regulation of angiogenesis	1.69E-05

D.

	Gene Ontology pathways	p. adjusted
GO:0016054	organic acid catabolic process	4.8E-06
GO:0009063	cellular amino acid catabolic process	2.1E-05
GO:0033539	fatty acid beta-oxidation using acyl-CoA dehydrogenase	6.9E-03
GO:0009083	branched-chain amino acid catabolic process	1.1E-02
GO:0055114	oxidation-reduction process	1.3E-02
GO:0006635	fatty acid beta-oxidation	1.3E-02
GO:0071346	cellular response to interferon-gamma	3.6E-03
GO:0035458	cellular response to interferon-beta	3.9E-03
GO:0002495	antigen processing and presentation of peptide antigen via MHC class II	6.9E-03
GO:0050870	positive regulation of T cell activation	3.1E-02

Supplementary Fig. 3. Liver neutrophils acquire an altered phenotype in chronic liver damage. (A) Heat map of the top-50 differentially expressed genes between liver and circulating neutrophils in DDC mice. **(B)** String analysis of top-50 differentially expressed genes. Only connected nodes are represented in the network. Genes corresponding to *Cellular response to polysaccharide* (GO 0071222) are shown in red. **(C).** Gene ontology enriched pathways in DDC-liver neutrophils when compared to control liver neutrophils. **(D).** Gene ontology

enriched pathways in control liver neutrophils when compared to DDC-liver neutrophils.

A.

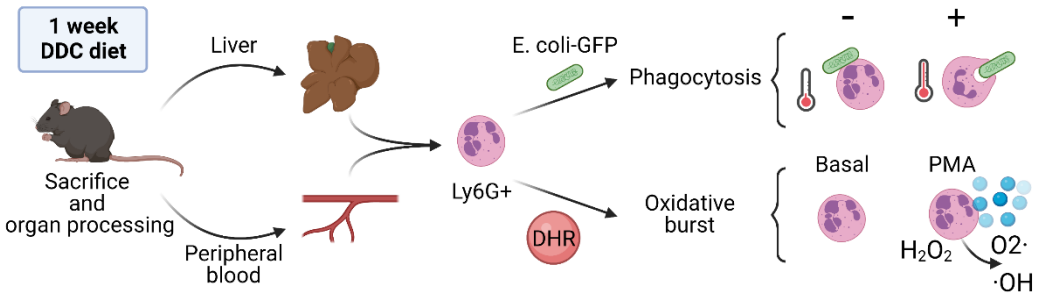

Supplementary Fig. 4. Liver neutrophils present an altered functionality. (A) Graphical scheme of phagocytosis and oxidative burst assessment in liver and circulating neutrophils isolated from 1-week treated DDC mice.

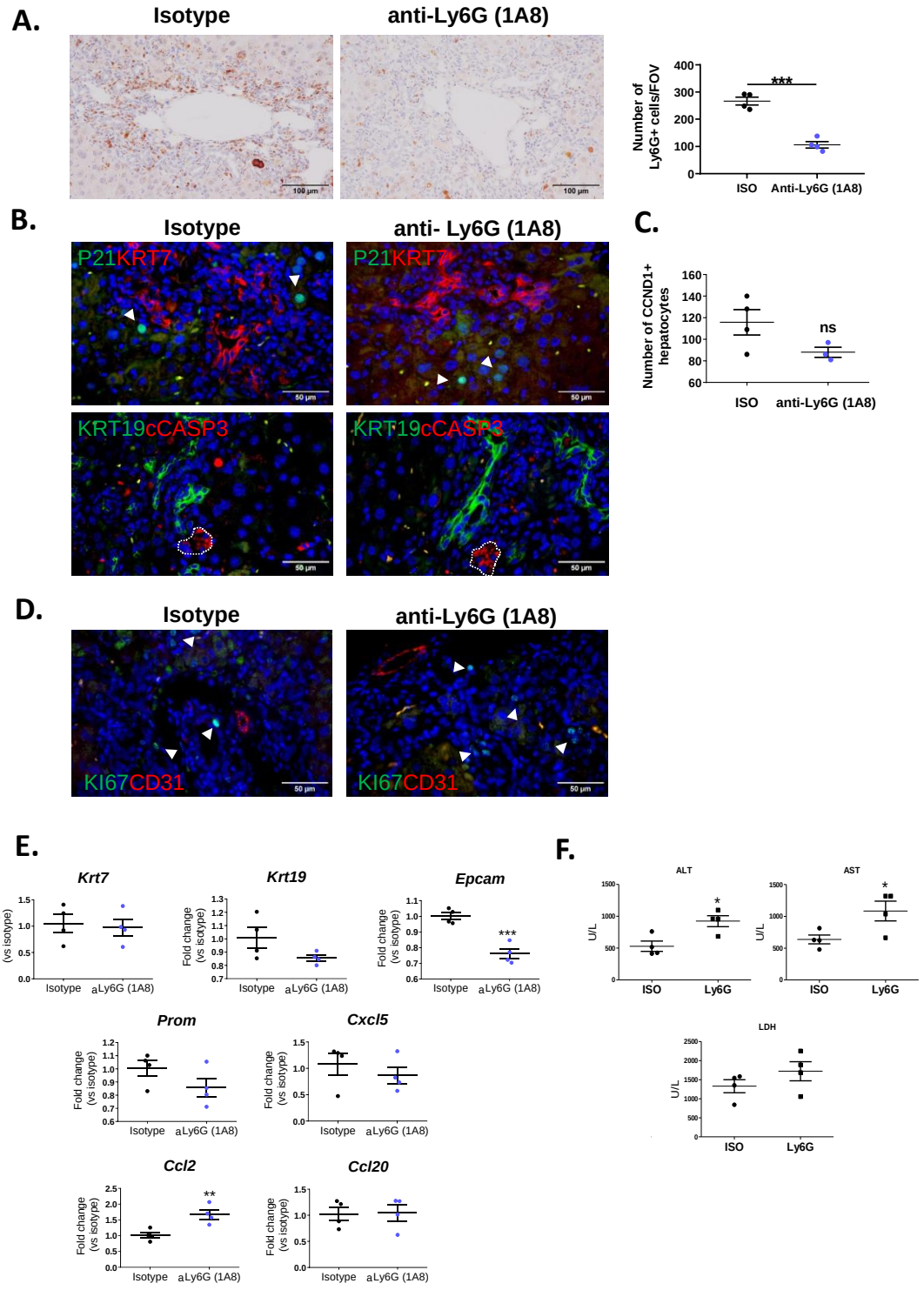

Supplementary Fig. 5. Neutrophil depletion impacts ductular reaction expansion in chronic liver injury. As a depletion model, mice were treated with αLy6G (1A8) antibody or isotype (500µg each, n=4 mice per group) together with DDC diet for 3 weeks. **(A)** Representative immunohistochemistry of Ly6G. Quantification of manually counted Ly6G+ cells per field of view (FOV) is shown.

(B) Representative immunofluorescence images of senescence (P21) and apoptosis (cleaved caspase 3 (cCASP3)) markers together with KRT7 in anti-Ly6G and isotype treated groups. Arrows point senescent nuclei (P21) and dashed lines marks apoptotic areas (Ccasp3). Scale bars: 50 µm. **(C)** Quantification of the number of Cyclin D1 (CCND1) positive hepatocytes per FOV. **(D)** Representative staining of KI67 and the endothelial cell marker CD31. Scale bars: 50 µm. **(E)** Gene expression analysis of progenitor cells (*Krt7, Krt19, Epcam, Prom*) and inflammation (*Ccl2, Ccl20, Cxcl5*) markers. **(F)** Serum levels of alanine aminotransferase (ALT), aspartate aminotransferase (AST) and lactate dehydrogenase (LDH). Data presented as mean ± SEM. *p<0.05, **p<0.01, ***p<0.0001, ns: non-significant, as determined by Unpaired t-test.

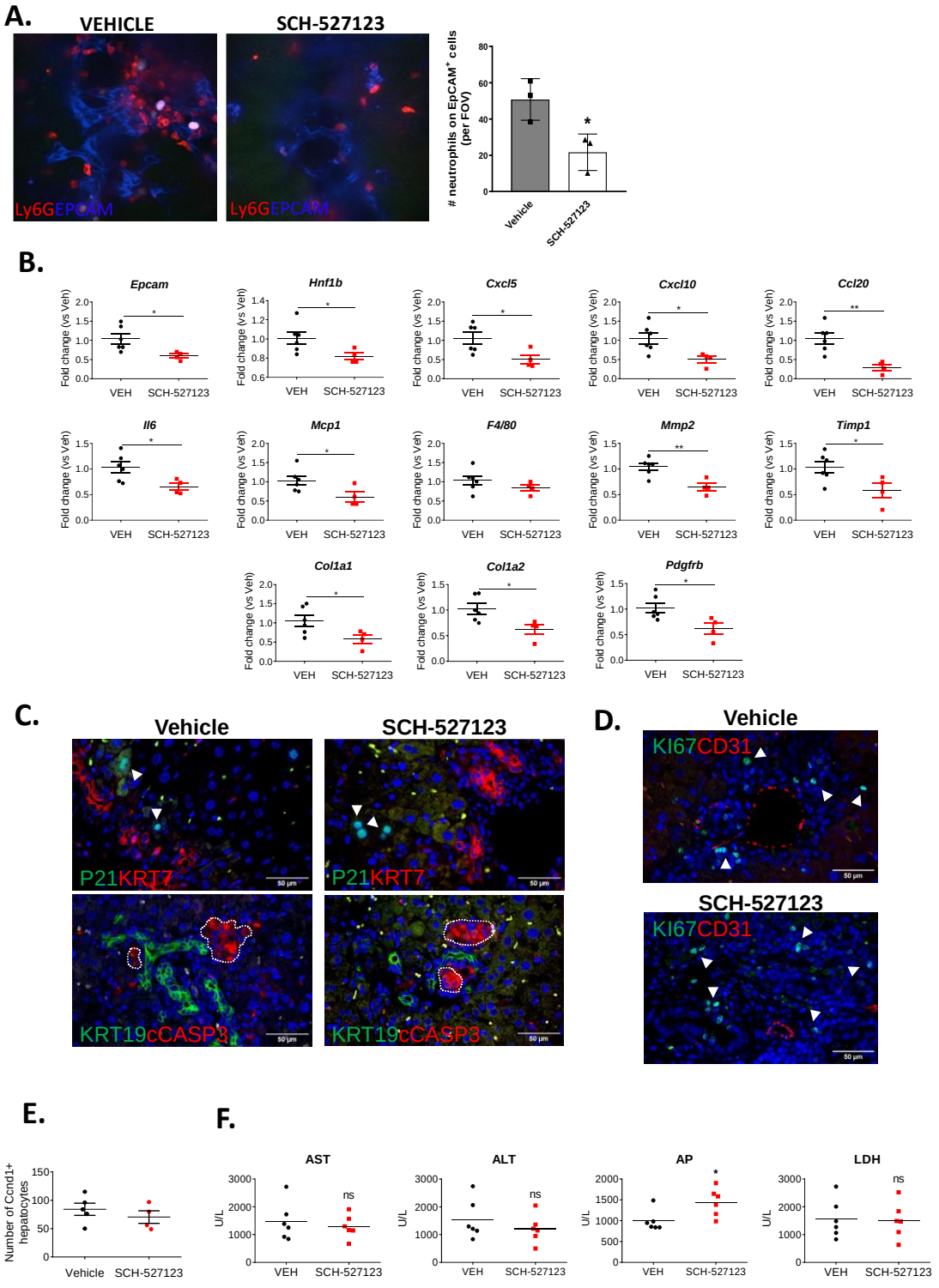

Supplementary Fig. 6. Long-term inhibition of neutrophil recruitment attenuates liver injury in DDC-induced chronic injury. First, mice were simultaneously fed with DDC and daily treated with vehicle or CXCR1/2 inhibitor (50mg/Kg) for 3 weeks (n=4-6 mice per group). **(A)** Representative SD-IVM images of DRANs recruited at the portal injury site (EpCAM$^+$ cells) in mice

receiving DDC for 1 week and treated with CXCR1/2 inhibitor (SCH-527123) or vehicle. Quantification of neutrophils recruited at biliary epithelium in both groups is shown. Each symbol represents a field of view (FOV). **(B)** Whole liver gene expression analysis of key markers of inflammation (*Cxcl5, Ccl20, Il6, Mcp1, F4/80, Cxcl10*), fibrosis (*Timp1, Col1a1, col1a2, Mmp2, Pdgfrb*) and DR (*Epcam, Hnf1b*) from mice treated with the inhibitor or vehicle (n=4-6 mice per group) for 3 weeks. **(C)** Representative immunofluorescence images of senescence (P21) and apoptosis (cleaved caspase 3 (cCASP3)) markers together with KRT7 in SCH-527123 and vehicle groups. Arrows point senescent nuclei (P21) and dashed lines marks apoptotic areas (cCASP3). Scale bars: 50 μm. **(D)** Representative staining of KI67 and the endothelial cell marker CD31. Scale bars: 50 μm. **(E)** Quantification of the number of Cyclin D1 (CCND1) positive hepatocytes per FOV. **(F)** Serum levels of ALT, AST, AP and LDH in both groups. Data presented as mean ± SEM. *p<0.05, **p<0.01, ns: non-significant, as determined by Unpaired t-test (A, B, AST, ALT and LDH in C) and Mann-Whitney test (AP in C).

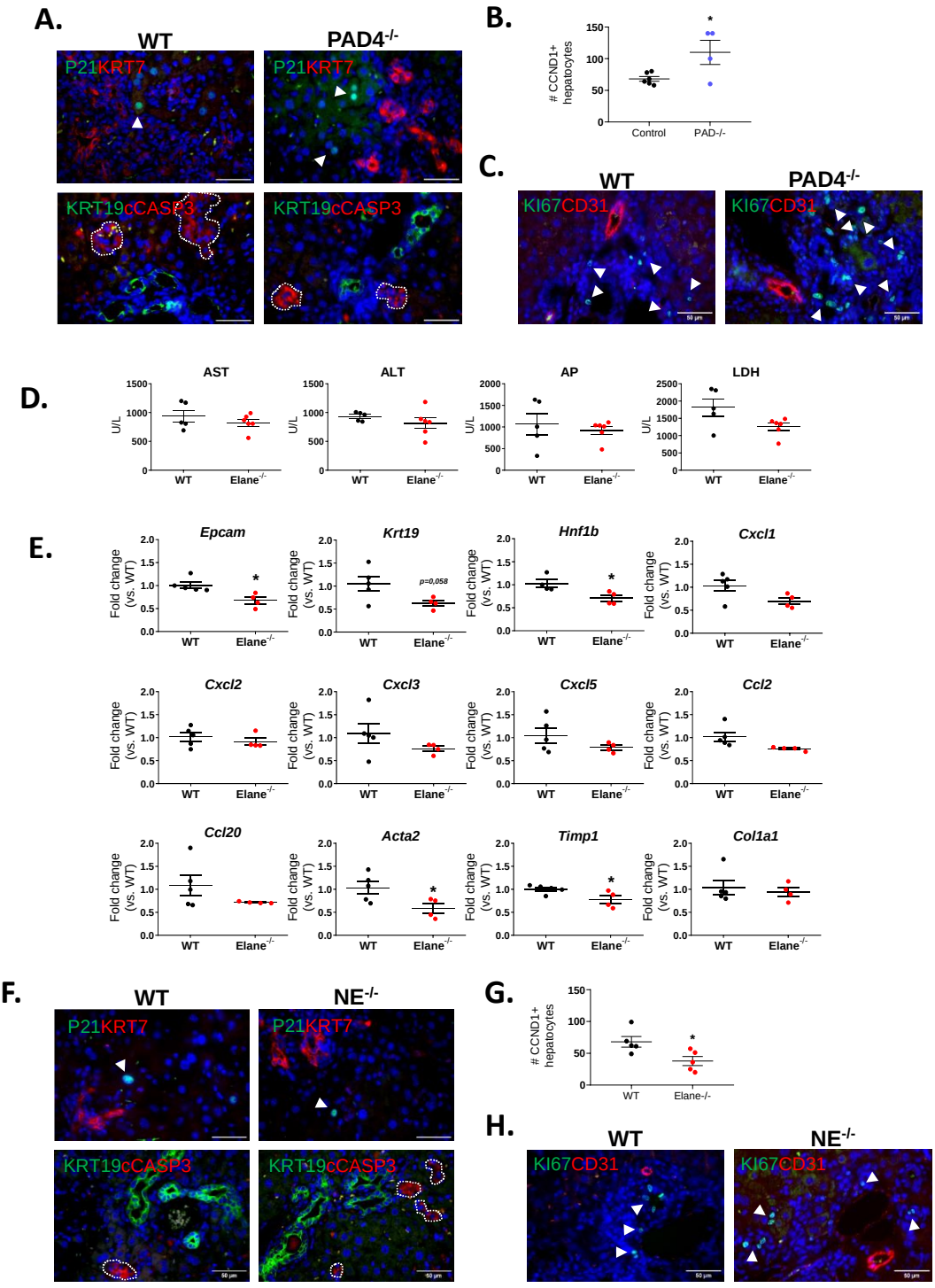

Supplementary Fig. 7. Absence of elastase release ameliorates biliary progenitor cell expansion. (A) Representative immunofluorescence images of senescence (P21) and apoptosis (cleaved caspase 3 (cCASP3)) markers together with KRT7 in WT and PAD4$^{-/-}$ mice treated with DDC for 3 weeks. Arrows point senescent nuclei (P21) and dashed lines marks apoptotic areas (cCASP3). Scale bars: 50 µm. **(B)** Quantification of the number of Cyclin D1 (CCND1)

positive hepatocytes per FOV. **(C)** Representative staining of KI67 and the endothelial cell marker CD31. Scale bars: 50 µm. **(D)** Serum levels of ALT, AP, AST and LDH. **(E)** Whole liver gene expression analysis of biliary/progenitor (*Hnf1β, Krt19, Epcam*), inflammation (*Ccl2, Ccl20, Cxcl5, Cxcl3, Cxcl2, Cxcl1*) and fibrosis (*Acta2, Timp1, Col1a1*) markers. **(F)** Representative immunofluorescence images of senescence (P21) and apoptosis (cleaved caspase 3 (cCASP3)) markers together with KRT7 in WT and $NE^{-/-}$ mice treated with DDC for 3 weeks. Arrows point senescent nuclei (P21) and dashed lines marks apoptotic areas (cCASP3). Scale bars: 50 µm. **(G)** Quantification of the number of Cyclin D1 (CCND1) positive hepatocytes per FOV. **(H)** Representative staining of KI67 and the endothelial cell marker CD31. Scale bars: 50 µm. Data is presented as mean ± SEM. *p<0.05 as determined by Unpaired t-test.

Supplementary Videos data legends

Supplementary movie 1. Chronic liver injury results in neutrophil recruitment at human biliary epithelium. Representative video of neutrophils (MPO) recruited to biliary epithelium cells (KRT7) in a cleared liver sample of a patient with chronic liver injury.

Supplementary movie 2. Interaction of DRANs with ductular reaction cells in mice receiving DDC for 1 week. 3D reconstruction demonstrates that neutrophils (Ly6G) directly interact with ductular reaction cells (KRT7).

Supplementary movie 3. Static behavior of DRANs in mice receiving DDC for 1 week: Intra-vital visualization of the static behavior of neutrophils (Ly6G) recruited at the biliary epithelium (EpCAM).

Supplementary movie 4. Static behavior of DRANs attached to biliary epithelium in mice receiving DDC for 1 week and subjected to focal thermal injury: Intravital visualization showing that neutrophils retained at ductular reaction structures are not mobilized towards a sterile (acute) injury. Video was recorded in DDC mice at 24 hours after focal thermal injury.

Supplementary References

[1] Swamydas M, Luo Y, Dorf ME, Lionakis MS. Isolation of Mouse Neutrophils. Curr Protoc Immunol 2015;110:3.20.1-3.20.15. https://doi.org/10.1002/0471142735.IM0320S110.

[2] Renier N, Wu Z, Simon DJ, Yang J, Ariel P, Tessier-Lavigne M. iDISCO: A Simple, Rapid Method to Immunolabel Large Tissue Samples for Volume Imaging. Cell 2014;159:896–910. https://doi.org/10.1016/J.CELL.2014.10.010.

[3] Mócsai A, Zhang H, Jakus Z, Kitaura J, Kawakami T, Lowell CA. G-protein–coupled receptor signaling in Syk-deficient neutrophils and mast cells. Blood 2003;101:4155–63. https://doi.org/10.1182/blood-2002-07-2346.

[4] Dobin A, Gingeras TR. Mapping RNA-seq Reads with STAR. Curr Protoc Bioinformatics 2015;51:11.14.1. https://doi.org/10.1002/0471250953.BI1114S51.

[5] Li B, Dewey CN. RSEM: accurate transcript quantification from RNA-Seq data with or without a reference genome. BMC Bioinformatics 2011;12:1–16. https://doi.org/10.1186/1471-2105-12-323.

[6] Law CW, Chen Y, Shi W, Smyth GK. voom: precision weights unlock linear model analysis tools for RNA-seq read counts. Genome Biol 2014;15:1–17. https://doi.org/10.1186/GB-2014-15-2-R29.

[7] Smyth GK. limma: Linear Models for Microarray Data. Bioinforma Comput Biol Solut Using R Bioconductor 2005:397–420. https://doi.org/10.1007/0-387-29362-0_23.

[8] Broutier L, Andersson-Rolf A, Hindley CJ, Boj SF, Clevers H, Koo BK, et al. Culture and establishment of self-renewing human and mouse adult liver and pancreas 3D organoids and their genetic manipulation. Nat Protoc 2016;11:1724–43. https://doi.org/10.1038/nprot.2016.097.